Proceedings of the CAS–CERN Accelerator School: Beam Injection, Extraction and Transfer, Erice, Italy, 10-19 March 2017, edited by B. Holzer, CERN Yellow Reports: School Proceedings, Vol. 5/2018, CERN-2018-008-SP (CERN, Geneva, 2018)

Fast Extraction: Single and Multiturn

M.A. Fraser
CERN, Geneva, Switzerland

Abstract
The basic principles and design considerations for fast extraction systems are introduced and reviewed before examples of CERN systems are given to illustrate different techniques. Single-turn fast extraction is used to introduce the main concepts before an overview of multiturn fast extraction techniques, including mechanical and magnetic beam splitting, is presented.

Keywords
Fast extraction; continuous transfer; CT; multiturn extraction; MTE.

1 Introduction

In many ways, extraction is simply the reverse process of injection; however, extraction is usually made after acceleration and therefore at higher energy, requiring stronger elements. As a result, many kicker and septum modules may be required; space–charge effects are usually less of a concern but beam losses, induced radio-activation, and machine protection considerations are typically more important. Different extraction techniques from synchrotrons exist, depending on the given requirements:

1. fast single-turn extraction ($\leq$1 turn): e.g., transfer between machines in an accelerator complex, transfer to experimental (production) targets or to safely dump the circulating beam (fast abort);
2. fast multiturn extraction (a few turns): to uniformly fill a synchrotron with a larger circumference or to vary the spill length to experimental targets over a few turns;
3. slow resonant multiturn extraction (many thousands of turns): providing experimental target, or patient, with long uniform spills;
4. other exotic extraction types, such as with bent crystals or charge-exchange extraction.

In this contribution, only items 1 and 2 will be discussed in detail. More details on items 3 and 4 can be found in the dedicated contributions made elsewhere in these proceedings.

Nowadays, extraction systems are usually considered from the conception of an accelerator, but this was not always the case in the past because lower stored beam energies and intensities meant that machine protection and radio-protection considerations were less of a concern. Consideration of the extraction system is a necessity during the conception of high-momentum machines, such as the Super Proton Synchrotron (SPS) or Large Hadron Collider (LHC) at CERN, where the layout, performance, and protection of the synchrotron might be significantly influenced by the design of the extraction system itself. A relevant example at present is the ongoing design work for the Future Circular Collider (FCC), where the extraction region is one of the most critical systems at the heart of the layout and lattice considerations [1]. The main considerations for a general extraction system can be summarized as follows:

1. destination or user: e.g., precision of beam delivery, tolerated beam loss, or emittance blow-up;
2. beam optics, integration, aperture, interference, and interplay with other essential subsystems: e.g., insertion regions may be required to meet specific requirements;
3. failure scenarios and their mitigation: e.g., at high energy or intensity, the extraction (beam-dump) system becomes an integral part of the machine protection system.

https://doi.org/10.23730/CYRSP-2018-005.285

All of these considerations affect the choice of hardware employed for any given application, leading to an iterative design process involving many subsystems of the accelerator. To satisfy all of these constraints, one might require the extraction system to be placed in a dedicated insertion region that breaks the regular lattice structure of the synchrotron. The archetypal extraction system where machine protection concerns overshadow the design would be the LHC beam-dump system [2].

2 Single-turn fast extraction

A classical fast extraction system consists of a fast-pulsed kicker (magnetic or electric) that deflects the circulating beam over the septum blade and into the high-field region of a septum magnet located at a suitable phase advance downstream, as described in Fig. 1. A local, closed-orbit bump is used to reduce the kicker strength required to jump the septum blade. As shown in the inset in Fig. 1, the field pulse of the kicker rises synchronously with a particle-free gap in the circulating beam to avoid sweeping the beam over the septum blade. For extraction over a single turn, the length of the kicker pulse should exceed the length of the circulating bunch train, or the revolution period of the synchrotron.

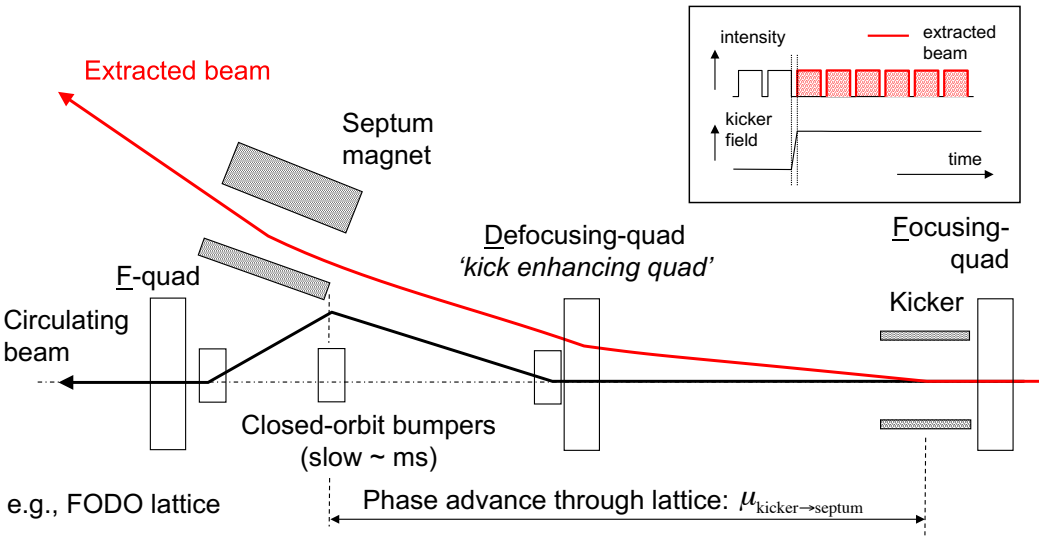

Fig. 1: Classical fast extraction system

2.1 Kick dynamics

The defocusing quadrupole placed between kicker and septum, often termed a kick enhancement quadrupole, can be seen as helping to deliver the phase advance and enhancing the kick imparted by the kicker, as described by the commonly used expression

$$\Delta x_{\text{septum}} = \Delta x'_{\text{kicker}} \sqrt{\beta_{\text{kicker}} \beta_{\text{septum}}} \sin\left(\mu_{\text{kicker}\to\text{septum}}\right) . \tag{1}$$

It is common to describe the kick strength in terms of the maximum number of beam widths of spatial separation developed downstream, which is why a normalized phase-space description becomes particularly useful. The beam width is often parametrized by a statistical quantity describing the distribution of the beam density, e.g., using the root-mean-square termed σ in the case of a Gaussian distribution. For a normalized deflection of $n\sigma$ at the kicker, one can write

$$\Delta x'_{\text{kicker}} = n\sqrt{\frac{\epsilon}{\beta_{\text{kicker}}}} \qquad \text{and} \qquad \Delta \bar{X}'_{\text{kicker}} = n\sqrt{\epsilon} \, , \tag{2}$$

such that the spatial separation at the septum located at a phase advance $\Delta\mu$ downstream can be expressed as

$$\Delta x_{\text{septum}} = n\sqrt{\epsilon\beta_{\text{septum}}}\sin\Delta\mu \qquad \text{and} \qquad \Delta\bar{X}_{\text{septum}} = n\sqrt{\epsilon}\sin\Delta\mu\ , \tag{3}$$

where the 1σ beam emittance is defined by

$$\epsilon = \frac{\sigma^2}{\beta}. \tag{4}$$

The separation in normalized phase-space created by the kicker, at both its location and the downstream septum, is shown schematically in Fig. 2, where the particular normalization $(x, x') \rightarrow (\bar{X}, \bar{X}')$ is the same as that presented in the 'Introduction to beam transfer' paper of these proceedings.

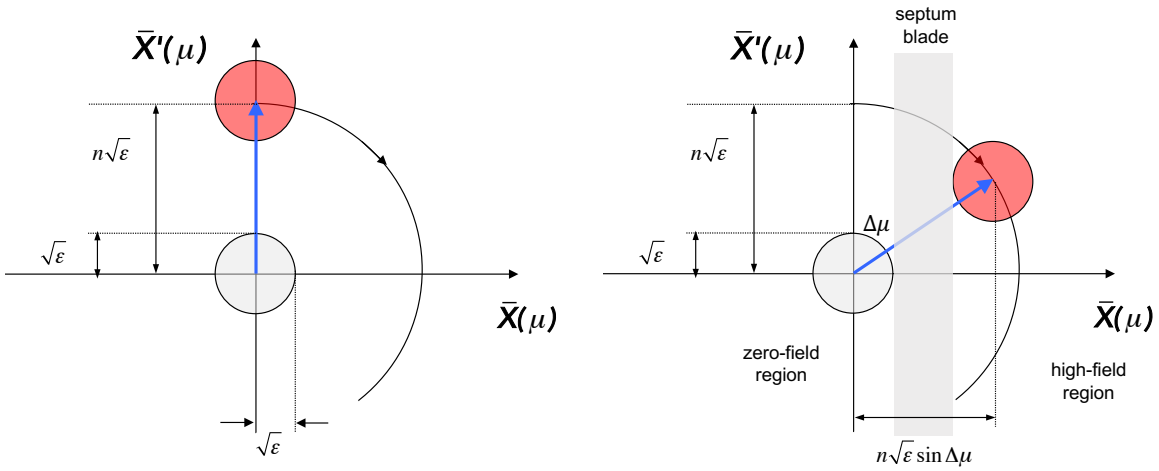

(a) At the kicker

(b) At a septum located at a phase advance $\Delta\mu$ downstream

Fig. 2: Extraction kick dynamics in normalized phase-space developing an opening of $n\sigma$ between the extracted (red) and circulating (grey) beams, where $\epsilon = \sigma^2/\beta$.

There is no strong constraint on the distance between kicker and septum, as long as the phase advance is chosen so that spatial separation is achieved. As a result, it is not uncommon to see kickers and septa separated by large distances around a synchrotron or to find the kicker deflecting in the opposite direction to the septum, i.e., kicking to the inside of the ring to extract via a septum on the outside. For septa located on the outside of the ring, i.e., for $x > 0$ and maximal separation, one can write:

$$\Delta x_{\text{septum}} = \underbrace{(-1)^{m-1}|\Delta x'_{\text{kicker}}|}_{\Delta x'_{\text{kicker}}}\sqrt{\beta_{\text{kicker}}\beta_{\text{septum}}}\sin\left(\mu_{\text{kicker}\rightarrow\text{septum}}\right)\ , \tag{5}$$

where

$$\mu_{\text{kicker}\rightarrow\text{septum}} = \frac{2m-1}{2}\pi \quad \text{for} \quad m = 1, 2, 3, \ldots \tag{6}$$

A single kicker system can service a number of extraction channels, with septa located at different positions in the ring. The desired extraction channel can be selected by setting the kicker polarity and energizing the relevant extraction bump. Operation of a single kicker system can reduce the cost and maintenance of running several extraction beam lines and reduce the impedance that multiple systems would present to the beam. However, a reduced acceptance and stability of the extracted beam can be expected. The layout of the fast extraction systems and beam lines installed in the CERN Proton Synchrotron (PS) over the years was designed with such considerations in mind [3]. The effect of non-local

fast extraction on beam quality in a large high-energy synchrotron is detailed in Ref. [4]. An extreme case of non-local extraction can be found in Ref. [5], where a crystal was used to deflect protons over the septum and into the extraction channel after a journey of 1.5 turns in the synchrotron, making almost 41 betatron oscillations.

From the simple relationship in Eq. 1, it is obvious that, to minimize the kick strength required, a designer would aim at maximizing the β-functions at the locations of the kicker and septum, and optimize the phase advance between those locations. The importance of a large β-function at the kicker is shown intuitively in Fig. 3, where the separation between the extracted and circulating beams is given for two extreme cases but the same kick angle. When the beam divergence is small, less angular deflection is needed to 'jump' outside the circulating beam. It is interesting to note that the large-β condition is exactly the worst case for emittance growth arising from imperfections in the uniformity of the kicker pulse, which is, in many ways, analogous to emittance growth in thin foils (or scatterers).

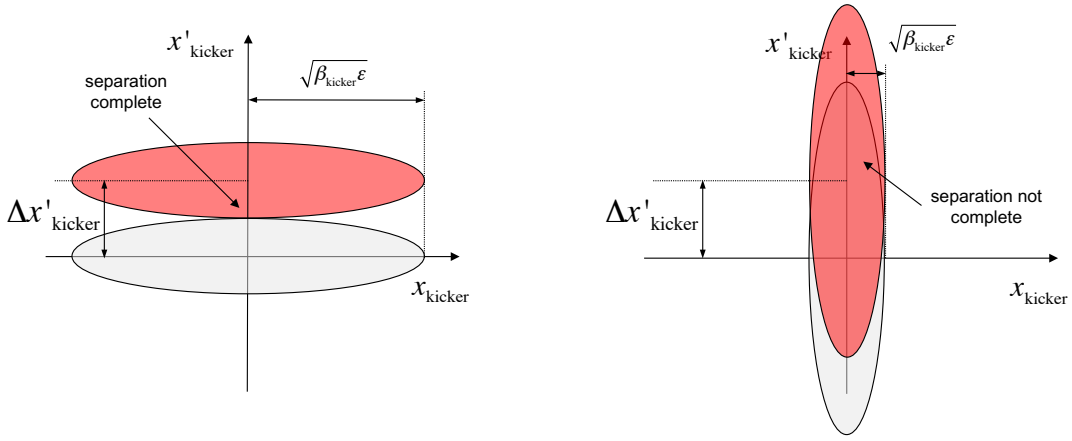

(a) Large β_{kicker}, assuming $\alpha_{\text{kicker}} = 0$

(b) Small β_{kicker}, assuming $\alpha_{\text{kicker}} = 0$

Fig. 3: Intuitive schematic example, demonstrating the advantage of a large β-function at the kicker

A similar argument can be made to explain why the β-function should also be large at the septum. One finds that, for a given kick angle, the separation, and therefore the maximum septum blade thickness that can be used, is proportional to $\sqrt{\beta_{\text{septum}}}$. Typically, the thicker the blade, the easier the engineering of the septum.

2.1.1 Kicker design parameters

The main considerations are typically rise and fall time, flat-top ripple, or field uniformity along the pulse and post-pulse ripple, depending on the particular application. The rise and fall times are usually defined between given limits of the nominal field, e.g., 2–98%, and the ripple in units relative to the nominal field. The typical figures of merit used to set tolerances for these design parameters are the acceptable beam emittance growth and beam loss. Three examples are given in Fig. 4 for the following applications:

- transfer between injectors in an accelerator complex for a high-energy collider: emittance conservation of extracted beam is of maximum importance, low flat-top ripple and fast rise times are needed;
- transfer for fixed-target physics in multiburst mode: perturbing the circulating beam might induce blow-up and losses of the circulating beam, fast rise or fall times and low post-pulse ripple are needed;

– fast beam abort to external absorber: safe, low-loss extraction of the circulating beam is important, flat-top ripple is relevant only for aperture reasons as emittance growth is not a consideration.

The expected perturbation imparted on the beam in the examples shown in Figs. 4(a) and 4(b) can be computed by taking the time-dependent waveform, applying the kick along a simulated bunch distribution and assuming complete filamentation in the receiving machine, see e.g., Ref. [6]. A transverse damper and feedback system in the receiving machine may be able to correct the time-correlated angular distortions introduced by the extraction kicker and reduce the emittance growth. In the case of the beam abort system shown in Fig. 4(c), flat-top ripple may be introduced deliberately to dilute the beam energy density on the dump absorber to an acceptable level that also guarantees transmission through the extraction channel and external beam line. Further details of beam dilution by fast-pulsed kickers for the SPS and LHC fast beam abort systems can be found in Refs. [7, 8]. Another important parameter driving the kicker specification is the aperture or stay-clear distance required for the circulating beam.

2.1.2 Septum design parameters

Owing to the relative strength of septa, which are typically 10 times stronger than kickers, field homogeneity is a more important design consideration. Both field homogeneity and shot-to-shot jitter can affect the transfer and beam quality. Along with aperture constraints, the stray field seen by the circulating beam must also be taken into account.

2.1.3 Aperture considerations

The main concerns for the extraction aperture are beam-loss-induced heating (impact on cooling requirements) and radio-activation (maintenance or damage) of the septum. The aperture is usually written in terms of the betatron beam size, where, in the horizontal plane,

$$\sigma_x = \sqrt{K_\beta \beta_x \epsilon_x}\,, \tag{7}$$

where the symbols have their usual meaning and K_β is an optics safety factor, generally taken as ≈ 1.2. The bumped, circulating beam aperture can be written as

$$n_{\sigma_x,\,\text{bump}} = \frac{A_{\text{septum}} - x_{\text{bump}} - \delta_{\text{CO}} - \delta_{\text{align}} - (|\delta_p| + |\delta_{\Delta p}|)|D_x|K_\beta}{\sigma_x}\,, \tag{8}$$

where the variables are defined in Figs. 5 and 6, δ_{CO} is the maximum residual on the closed orbit, δ_{align} is the mechanical alignment tolerance of the septum position, and δ_p and $\delta_{\Delta p}$ are the maximum momentum error of the beam and its spread, respectively. Similarly, the extracted beam aperture can be written

$$n_{\sigma_x,\,\text{ext}} = \frac{\Delta x_{\text{septum}} + x_{\text{bump}} - (\Delta x_{\text{blade}} + A_{\text{septum}}) - \delta_{\text{CO}} - \delta_{\text{align}} - (|\delta_p| + |\delta_{\Delta p}|)|D_x|K_\beta}{\sigma_x}\,, \tag{9}$$

which is dependent on the strength of the kicker and the septum blade thickness. The vertical aperture for the extracted beam is usually critical because of the narrow septum gap height,

$$n_{\sigma_y} = \frac{y_{\text{gap}}/2 - \delta_{\text{CO}} - \delta_{\text{align}}}{\sigma_y}\,. \tag{10}$$

The extraction kicker is usually installed on the circulating beam trajectory; therefore, its gap height (vertical aperture) is constrained by the beam size at injection for a horizontal kicker, as shown in Fig. 5. The proximity of the extraction septum to the circulating beam is typically limited by the size of the beam, and therefore the machine acceptance, at injection, as shown in Fig. 6. Most synchrotrons serve a number of beam types and users; to avoid mechanically actuating the septum position to maximize the acceptance on a beam-by-beam basis, a closed-orbit bump is exploited. The septum is left mechanically

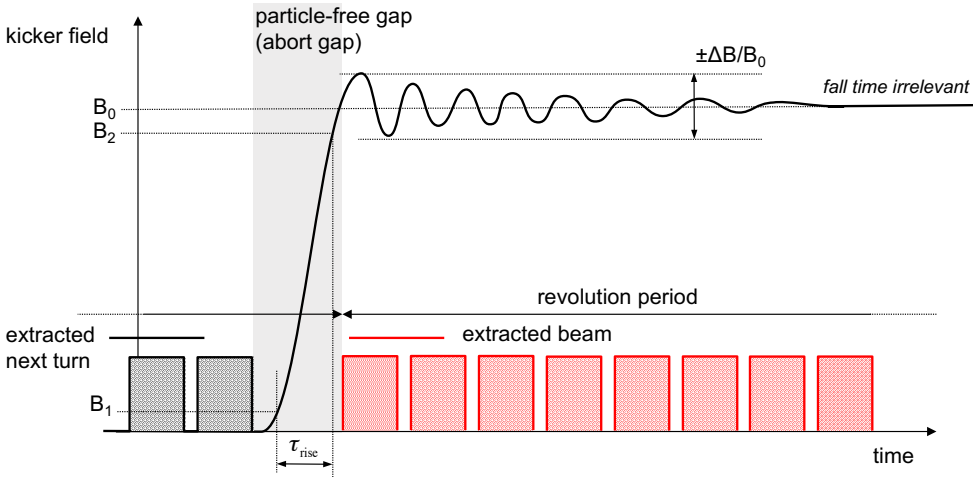

(a) Single-turn extraction between injectors in accelerator complex for high-energy collider

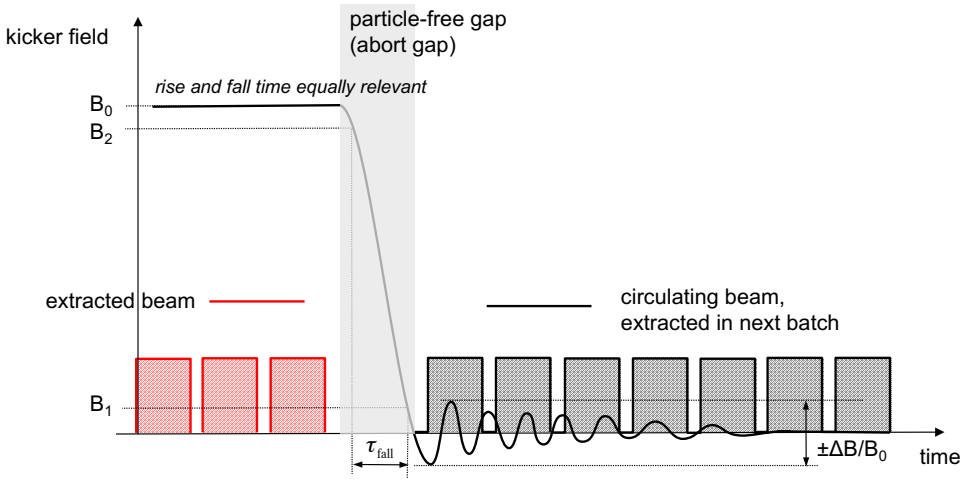

(b) Transfer for fixed-target physics in multiburst mode

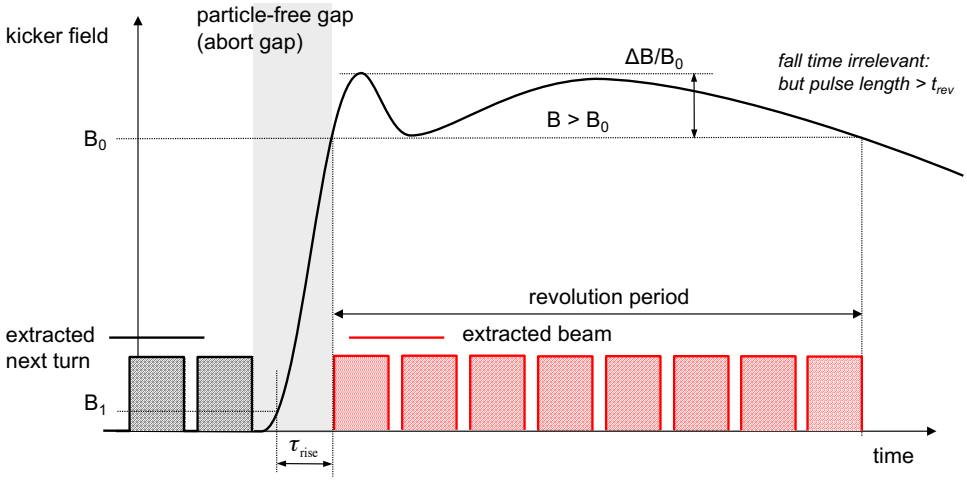

(c) Fast beam abort to external absorber

Fig. 4: Kicker waveforms, showing typical applications for fast extraction systems and relevant parameters

fixed outside of the machine acceptance and the accelerated beam is moved closer to the septum by the bump immediately before extraction. The aperture that can be gained is related to the adiabatic damping of the emittance during acceleration and the ratio of the relativistic factor, $\sqrt{\beta_{\mathrm{inj}}\gamma_{\mathrm{inj}}/\beta_{\mathrm{ext}}\gamma_{\mathrm{ext}}}$. Similar ideas have also been considered to reduce the required aperture of extraction kickers by bumping the beam into an open C-shaped geometry after acceleration, where the return conductor is hidden on the rear side of the ferrite yoke [9]. In this way, the gap height is reduced and the available kick strength for a given voltage is increased. Interestingly, the first kicker systems used in the PS had to be actuated into the beam after acceleration for exactly this reason [10].

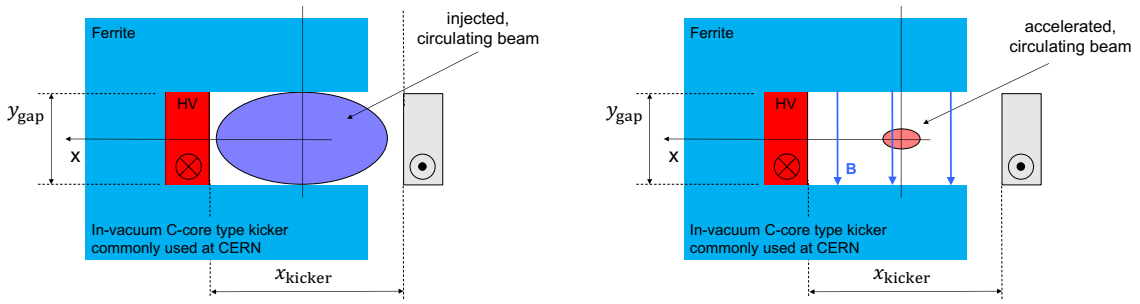

(a) At injection energy (b) At extraction energy, after acceleration

Fig. 5: Aperture considerations at the kicker for a fast extraction system

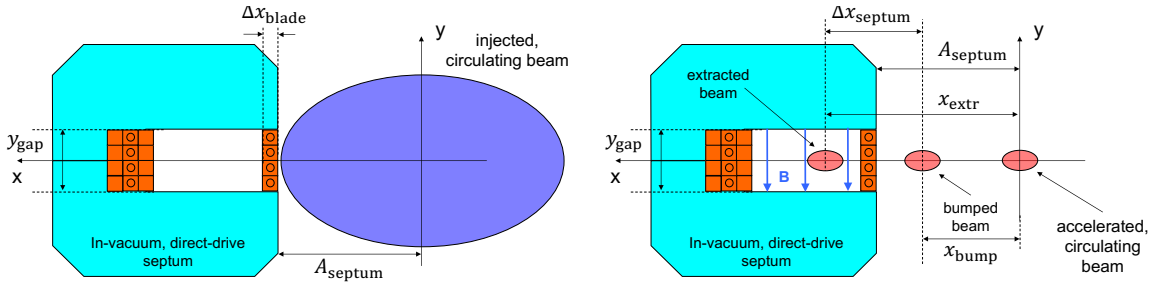

(a) At injection energy (b) At extraction energy, after acceleration

Fig. 6: Aperture considerations at the septum for a fast extraction system

2.1.4 Closed-orbit bumps

Closed-orbit bumps are regularly used during extraction to bring the circulating beam close to the septum (slow bump), to reduce the kicker strength, and to control multiturn extraction turn by turn (fast bump). Closed-orbit bumps are also commonly used for injection for similar purposes. Dipole 'bumper' magnets are used to steer the closed orbit away from the nominal trajectory in a localized part of the synchrotron. The following standard bump configurations exist and will be briefly discussed:

– π-bump;
– three- and four-magnet bumps.

The most important results needed for the implementation and design of closed-orbit bumps are quoted next. For further details and derivations, see Refs. [11, 12]. In reality, the analytical results presented next are rarely applicable to practical scenarios because there are usually far more constraints to consider. For such purposes, dedicated optics codes, e.g., MAD-X [13], are used to match bumps with numerical optimization routines.

2.1.4.1 π-bump

The simplest closed bump, the π-bump, is constrained by a phase advance of π or 180° between two dipole bumper magnets. As shown in Fig. 7, the first magnet opens the bump and the second closes it after half a betatron oscillation, where R is the linear transfer map describing the dynamics from one location to another along the accelerator. The relative deflection angle of the two bumpers is given by the lattice functions at the bumpers, as

$$\frac{\Delta_2}{\Delta_1} = \sqrt{\frac{\beta_1}{\beta_2}} \,. \tag{11}$$

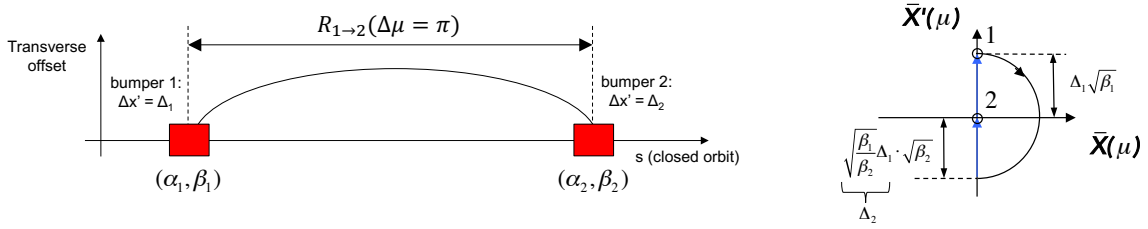

(a) Real space (x, s) along the reference trajectory

(b) Normalized phase-space $(\bar{X}, \bar{X}')$

Fig. 7: π-bump

2.1.4.2 *Three-magnet bump*

In a real accelerator, more degrees of freedom are often needed, for practical reasons. A third magnet can be added to close the bump for (almost) any value of phase advance between the first and last bumper. In this case, either the position or the angle can be matched at a location inside the bump. As shown in Fig. 8, the first and second bumpers put the beam back on the axis of the reference trajectory at the third bumper, which compensates for any remaining angle. The relative deflection angles of the bumpers can be written in terms of the lattice functions at the bumpers:

$$\frac{\Delta_2}{\Delta_1} = -\sqrt{\frac{\beta_1}{\beta_2}}\sqrt{\frac{\sin\Delta\mu_{13}}{\sin\Delta\mu_{23}}} \quad \text{and} \quad \frac{\Delta_3}{\Delta_1} = \sqrt{\frac{\beta_1}{\beta_3}}\left(\frac{\sin\Delta\mu_{13}}{\tan\Delta\mu_{23}} - \cos\Delta\mu_{13}\right) \,. \tag{12}$$

2.1.4.3 *Four-magnet bump*

To control both the position and angle at a given point S inside the bump, a fourth magnet is needed, see Fig. 9. The first two bumpers select the position and angle at a given location downstream of the

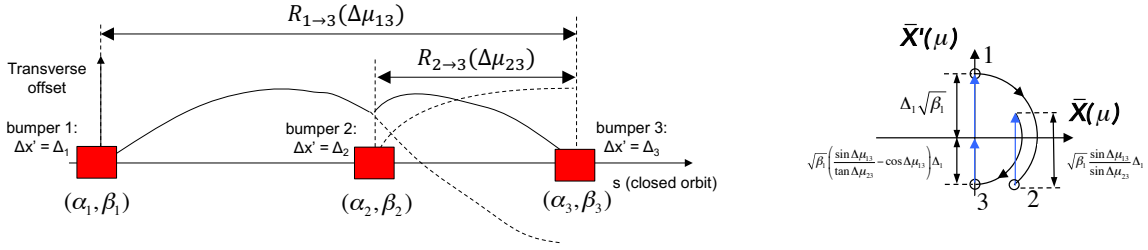

(a) Real space (x, s) along the reference trajectory

(b) Normalized phase-space $(\bar{X}, \bar{X}')$

Fig. 8: Three-magnet bump

second bumper, e.g., at the extraction septum, before two more bumpers return the beam to the reference trajectory. The relative deflection angles of the bumpers can be written in terms of the lattice functions at the bumpers and the matching point, as

$$\Delta_1 = -\frac{1}{\sqrt{\beta_1\beta_S}}\frac{\cos\Delta\mu_{2S} - \alpha_S\sin\Delta\mu_{2S}}{\sin\Delta\mu_{12}}x_S - \sqrt{\frac{\beta_S}{\beta_1}}\frac{\sin\Delta\mu_{2S}}{\sin\Delta\mu_{12}}x'_S \tag{13}$$

and

$$\Delta_2 = -\frac{1}{\sqrt{\beta_2\beta_S}}\frac{\cos\Delta\mu_{1S} - \alpha_S\sin\Delta\mu_{1S}}{\sin\Delta\mu_{12}}x_S + \sqrt{\frac{\beta_S}{\beta_2}}\frac{\sin\Delta\mu_{1S}}{\sin\Delta\mu_{12}}x'_S\,. \tag{14}$$

One can derive by symmetry the strengths of Δ_3 and Δ_4 by applying the following transformations to Eqs. (13) and (14):

$$\beta_1 \to \beta_4, \quad \beta_2 \to \beta_3, \quad \alpha_S \to -\alpha_S, \quad x_S \to -x_S, \quad \Delta\mu_{1S} \to \Delta\mu_{S4}, \quad \Delta\mu_{2S} \to \Delta\mu_{S3}\,. \tag{15}$$

The derivation of these relations is detailed at length in Ref. [11]. A useful application of the four-magnet bump is the construction of 'orthogonal bumps' to allow the independent variation of either the position or angle of the beam at a given location, whilst the other variable is held constant.

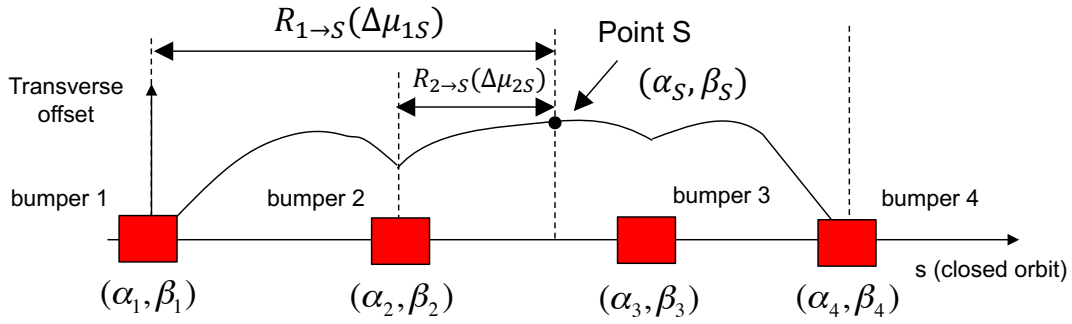

Fig. 9: Four-magnet bump in real space (x, s) along the reference trajectory

2.2 Example: fast extraction from SPS to LHC

The SPS fills the LHC with batches of high-brightness proton beams at a momentum of 450 GeV/c ($B\rho \approx 1500$ m) fast-extract over a single turn. The SPS has two fast extraction regions in Long Straight Sections (LSSs) 4 and 6 to fill the two counter-rotating LHC beams, as shown in Fig. 10.

We will consider LSS4, shown in the simplified layout of Fig. 11, in more detail, to explore an example of an operational fast extraction system. A full description of the system can be found in Ref. [15]. The optics in LSS4 are an extension of the SPS's periodic FODO structure with widened aperture quadrupoles (QA) and a closely symmetrical four-magnet (MP) bump. The extraction kicker (MKE) is located about 70° in phase advance upstream of the extraction septum (MSE) and both deflect towards the outside of the ring in the horizontal plane. The basic optics parameters describing the extraction system are summarized in Table 1. The bump amplitude is matched with a maximum displacement at the MSE. It is interesting to note the deflection of the closed orbit in the quadrupoles and how the trajectories contrast in the real and normalized co-ordinates shown in Fig. 11(a). The bump amplitude is non-zero in the MKE. The upstream ends of both the MKE and MSE systems are located close to focusing quadrupoles (QF), where the β-function is at its largest. The length of the MSE, consisting of six separate tanks, is impressive and consumes most of the half-period in which it is installed. The large-aperture quadrupoles have a window in the coil through which the extracted beam can pass unimpeded

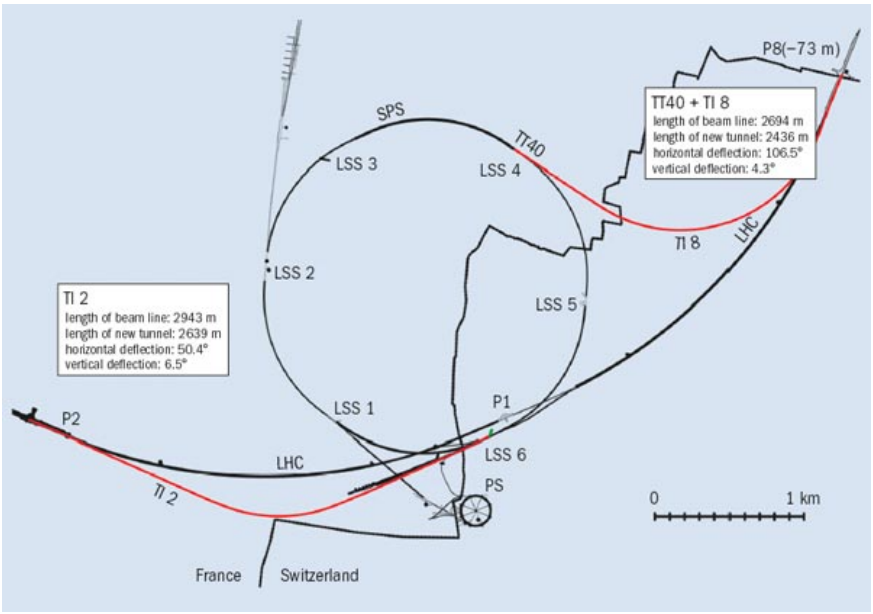

Fig. 10: SPS layout and LHC transfer lines: LSS4 (TI8) and LSS6 (TI2) [14]

to integrate an extraction beam line into the LSS. The passage of the extracted beam through the coil window of QDA.419 can be seen in Fig. 11(b). The position and angle of the MSE, the bump shape, and the bump shape amplitude are optimized with the aperture of the beam in mind. Approximately 10σ is available after acceleration for both the bumped and extracted beams.

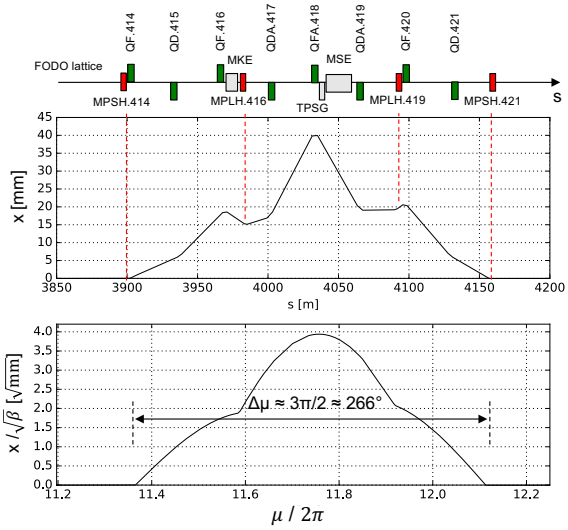

(a) Closed four-magnet bump trajectory

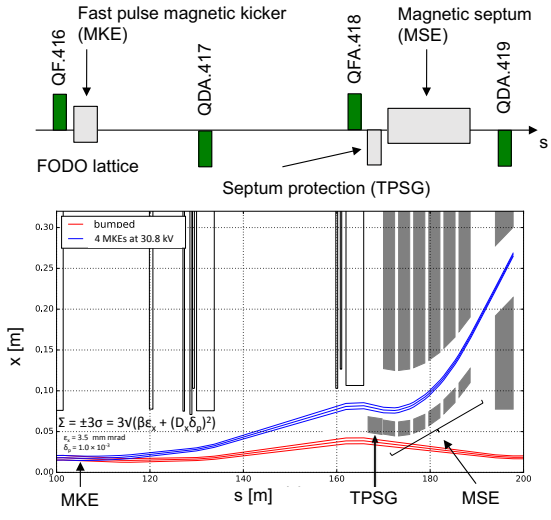

(b) Extraction channel aperture

Fig. 11: LSS4 fast extraction system for transfer from SPS to LHC

The stored energy of the beam at extraction amounts to close to 2.5 MJ and its brightness is high enough to damage the machine if mis-steered onto the aperture. To reduce the risk of failure and damage to the machine, a sophisticated interlock system is in place. As another level of protection against fast failure scenarios, which are difficult to detect and react to, such as a kicker flashing over as it pulses

Table 1: LSS4 optics parameters (given at upstream end of element)

Optics parameter	MKE	TPST	MSE	QF (QD)
β-function, β_x [m]	97.0	100.2	88.4	105 (32)
Phase advance, $\Delta\mu_x$ [degrees]	0	64.8	66.8	32
Deflection angle, $\Delta x'$ [mrad]	0.42	—	≈12	—

(potentially causing direct beam impact) or a kicker triggering erratically and asynchronously (causing the beam to sweep over the septum blade), a dedicated absorber or protection device (TPSG) is installed directly in front of the MSE to protect it. The TPSG is designed to survive a direct beam impact and is built from a sandwich of different materials to dilute the beam energy density sufficiently to avoid damage to the MSE [16].

3 Multiburst fast extraction

Multiburst fast extraction is demonstrated schematically in Fig. 12. It is essentially identical to single-turn fast extraction except that fast-pulsed kickers with short rise and fall times are used to extract part of the circulating beam by cutting-out 'bursts'. As discussed for the context of single-turn fast extraction, particle-free gaps must be present in the circulating beam, within which the extraction kicker system can pulse cleanly.

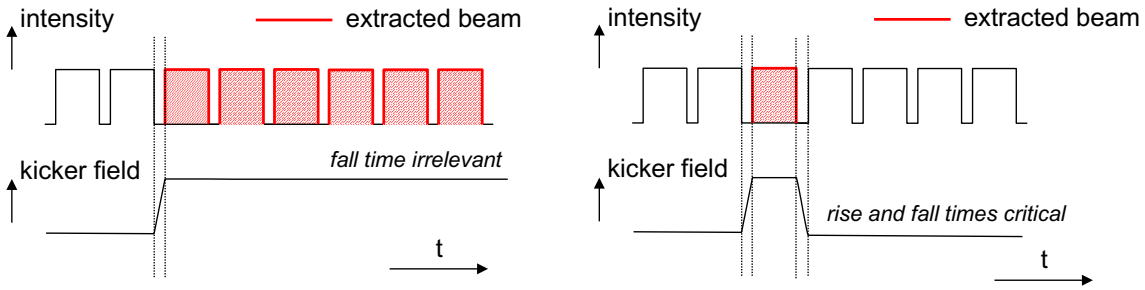

(a) Single-turn extraction (executed once)

(b) Multiburst extraction (repeated many times)

Fig. 12: Single-turn vs. multiburst extraction (time on horizontal axis)

An example of the multiburst fast extraction technique was the extraction of two bursts, separated in time by 50 ms (≈2000 turns), of approximately 2.5×10^{13} protons at 400 GeV from the SPS through LSS4 to the CERN Neutrino to Gran Sasso (CNGS) neutrino production target [17, 18]. In this case, the entire circumference of the SPS (23 µs) was filled by two batches, each 10.5 µs in length, injected from the PS and separated by approximately 1 µs. The circulating beam intensity around approximately half of the SPS ring is shown in Fig. 13, alongside the waveform of the kicker's current pulse. After acceleration and on the flat-top, a single fast extraction kicker system, recharged between bursts, was used to extract the two bursts into the extraction channel and towards the neutrino production target. In this case, two capacitor banks were used to resonantly and rapidly recharge the pulse-forming network. In reality, the particle-free gaps are not completely empty and a small amount of beam is lost during the extraction process, which, in this case, was estimated as a few tenths of one percent.

The total intensity that can be delivered by the synchrotron is limited by the presence of particle-free gaps and is dependent on the performance of the relevant kicker systems. Unless several extraction kicker systems are used and triggered independently, the repetition rate of the 'burst-mode' is typically limited by the need to recharge the kicker's power supply. An interesting application of burst-mode extraction is for the filling of a future high-energy collider, e.g., the FCC, where the amount of beam that can be transferred at once is limited by machine protection considerations, owing to the high beam

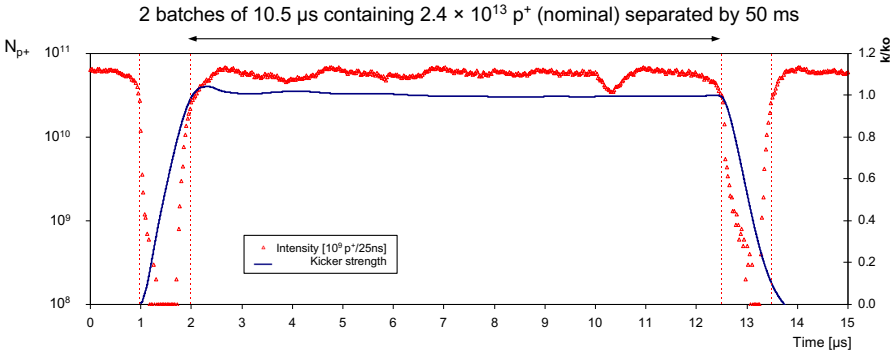

Fig. 13: Circulating CNGS beam intensity around approximately half of the SPS circumference, compared with the measured extraction kicker's current waveform [18].

energy and brightness [19]. To keep filling times reasonable, the filling pattern in the injector synchrotron and the design of its extraction system will have to be compatible with rapid pulsing in a burst-mode to empty the injector batch-by-batch safely and fill the collider efficiently.

Even by exploiting resonant charging from pre-charged capacitor banks, the time taken to recharge a pulsed-power supply, e.g., a pulse-forming network or pulse-forming line, is, in most cases, many times the revolution period. Installing more than one kicker system is challenging, owing to physical space constraints, or unfavourable, owing to the large beam impedance presented by kicker magnets. As a consequence, extracting in burst-mode very quickly over sequential turns, or at timescales close to the revolution period, becomes rather impractical. In applications where a continuous spill from the synchrotron is required over a few sequential turns, splitting of the beam must typically be carried out in the transverse plane; this is discussed next.

4 Multiturn fast extraction

To extend the spill length from a single turn to several turns of a synchrotron, one must consider separating or splitting the circulating beam in transverse phase-space whilst applying impulses on a turn by turn basis to extract the beam stepwise. When the energy and intensity of the circulating beam is high, a main challenge is the induced radio-activation of the accelerator and its extraction equipment, resulting from the loss of particles during the splitting and extraction processes. The fast and dynamic nature of the extraction process and resulting beam losses does not make it any easier to control. The impact of beam-induced radio-activation is particularly relevant at CERN, where fixed-target experimental facilities request upwards of 1×10^{19} protons on target per year at energies ranging from approximately 20 to 400 GeV. This has motivated significant developments for lower-loss multiturn extraction techniques at CERN over recent decades [20].

4.1 Non-resonant multiturn extraction: mechanical splitting

Non-resonant multiturn fast extraction by transverse shaving is a brute-force method employed to lengthen the spill from a synchrotron, which is useful for uniformly filling a larger downstream synchrotron and reducing the filling time, or for providing experiments with spills over a few turns. The concept is outlined in Fig. 14 and an example with a fractional tune of $q_{x,\mathrm{frac}} \approx 0.125$ is shown to illustrate the principle in Fig. 15. It can be instructive to see the process as reverse multiturn injection [21]. The circulating beam is shaved turn by turn on a thin electrostatic septum using a fast, programmable closed bump that forces the beam over the septum blade. The spatial separation required to extract the

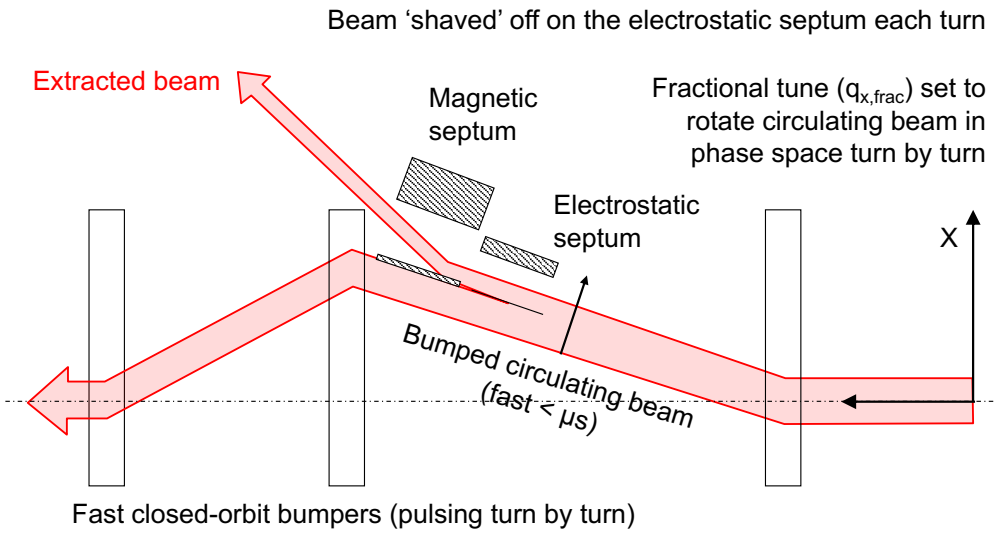

Fig. 14: Non-resonant multiturn extraction

beam from the synchrotron is created by cutting it on the thin septum blade, the deflection of the septum's electric field, and a non-zero phase advance to another, usually thicker, magnetic septum placed downstream. The tune of the synchrotron rotates the beam into the electrostatic septum to continuously shave the beam, turn by turn. If the circulating beam is debunched, the extracted spill will have a continuous time structure over the length of the spill, convoluted with the transverse beam density being shaved. The fractional part of the tune is adjusted, together with the height of the closed bump, to deliver the spill length desired.

As demonstrated in Fig. 15, the extraction process typically results in smaller beam emittances because the circulating beam is mechanically sliced in the plane of the extraction. This results in a spill with optical parameters that vary turn by turn and, as a consequence, the emittance, centroid position, and trajectory vary along the spill. It can be shown that, for realistic transverse beam distributions, spills with both uniform intensity and emittance are not possible [22].

The process is intrinsically lossy, as the septum blade directly intercepts the beam and, as a result, the accelerator is radio-activated by the extraction process. The extraction efficiency depends strongly on the number of turns extracted; therefore, it is seldom used to provide spills longer than ∼10–20 turns. This has limited its application at laboratories worldwide, especially for beam delivery to fixed-target experiments, although recently published beam tests at the U-70 synchrotron at IHEP describe the process and its challenges well [23]. Instead, resonant slow extraction can provide a more stable and efficient extraction mechanism, as described elsewhere in these proceedings, and can even be effective for relatively short spills of only ∼100 turns where the resonance is pulsed rapidly [24].

4.1.1 Continuous transfer at the CERN Proton Synchrotron

The term 'continuous transfer' (CT), as coined at the CERN PS [25], will be used synonymously with the expression 'non-resonant multiturn extraction' in these proceedings. Continuous transfer was developed to fill the larger SPS efficiently and uniformly for its fixed-target experimental programme, where the circumference of the SPS is approximately 11 times that of the PS. It should be noted that, in this case, uniform filling is of particular relevance for avoiding the onset of longitudinal instabilities in the SPS. The first versions of CT experimented with single-batch fills, with extractions over 10 and 11 turns from the

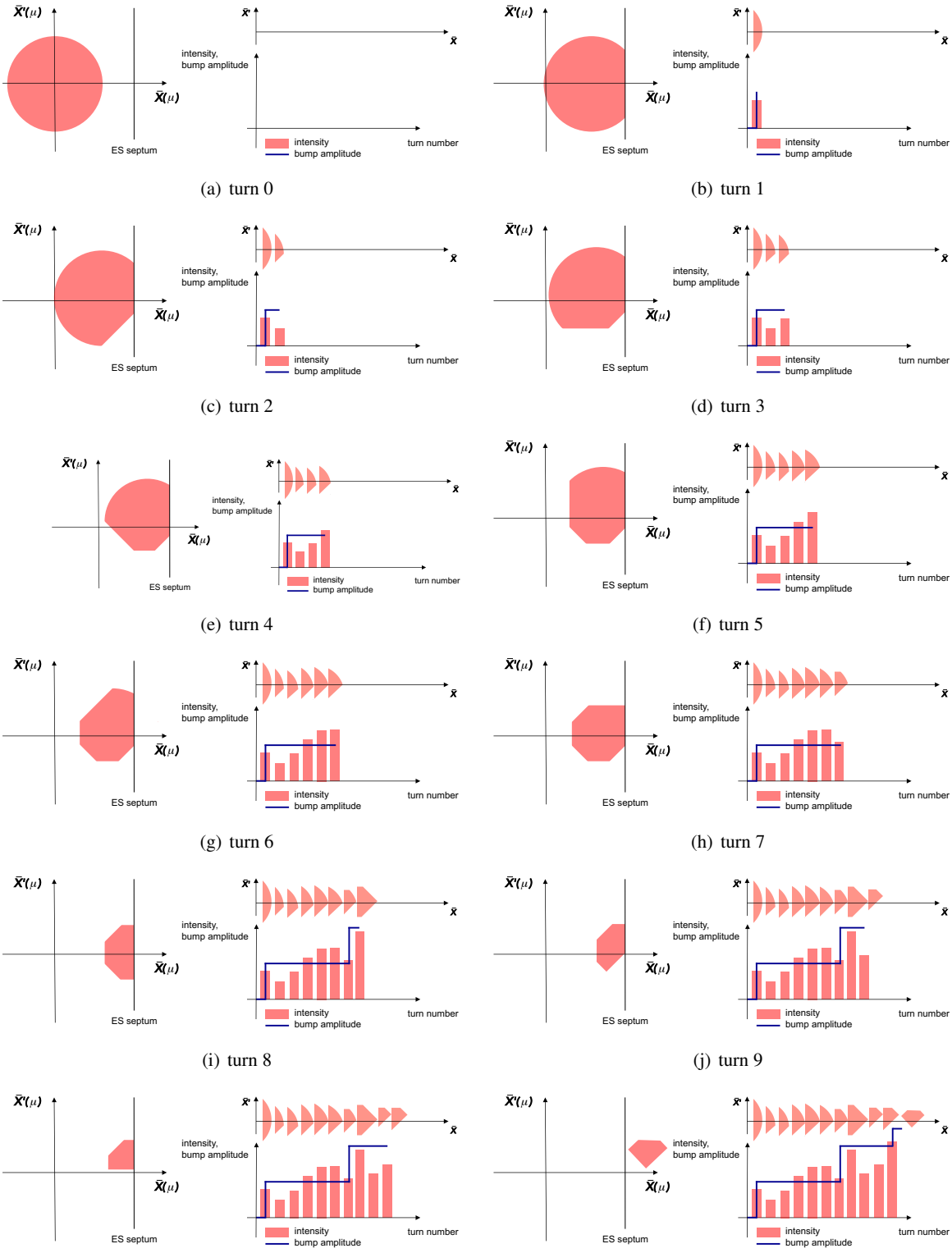

(a) turn 0

(b) turn 1

(c) turn 2

(d) turn 3

(e) turn 4

(f) turn 5

(g) turn 6

(h) turn 7

(i) turn 8

(j) turn 9

(k) turn 10

(l) turn 11

Fig. 15: Example of non-resonant multiturn extraction with fractional tune $q_{x,\text{frac}} \approx 0.125$.

PS, before the present-day double-batch scenario was developed (Fig. 16), which consists of the injection of two batches, each with a length of five PS turns. After acceleration and on the flat-top at 14 GeV/c the tune is brought close to $4Q_x = 25$. Slow, closed bumpers (BSW) bring the circulating beam close to the electrostatic (SEH31) and magnetic (SMH16) extraction septa before a fast-pulsed closed bump (BFA) around the electrostatic septum fires to commence the extraction. The beam is forced over the SEH31 blade, initiating the shaving. The deflection imparted by the SEH31 and the phase advance to SMH16 are such that the shaved slice is extracted into the transfer line as it passes the magnetic septum $\sim$500 m downstream. The tune rotates the beam over the subsequent four turns, continuously shaving the circulating beam before the fast bump amplitude increases further to push the remaining beam core out of the accelerator in the final turn. To reduce the density of the beam impinging the septum blade and enhance the deflection of the kickers and septa, a local, closed optics perturbation is applied between kick enhancement quadrupoles (QKE) during the extraction to increase the horizontal β-function at the SEH31. The closed QKE perturbation is also used to reduce the dispersion at SEH31 to ensure that the extraction is less sensitive to the momentum spread in the beam. Further details of the optics during the CT extraction can be found in Ref. [26]. To improve the RF capture in the SPS, the beam is debunched and partially recaptured at the SPS RF frequency of 200 MHz before extraction. A complete description of the CT extraction system at the PS can be found in Ref. [10].

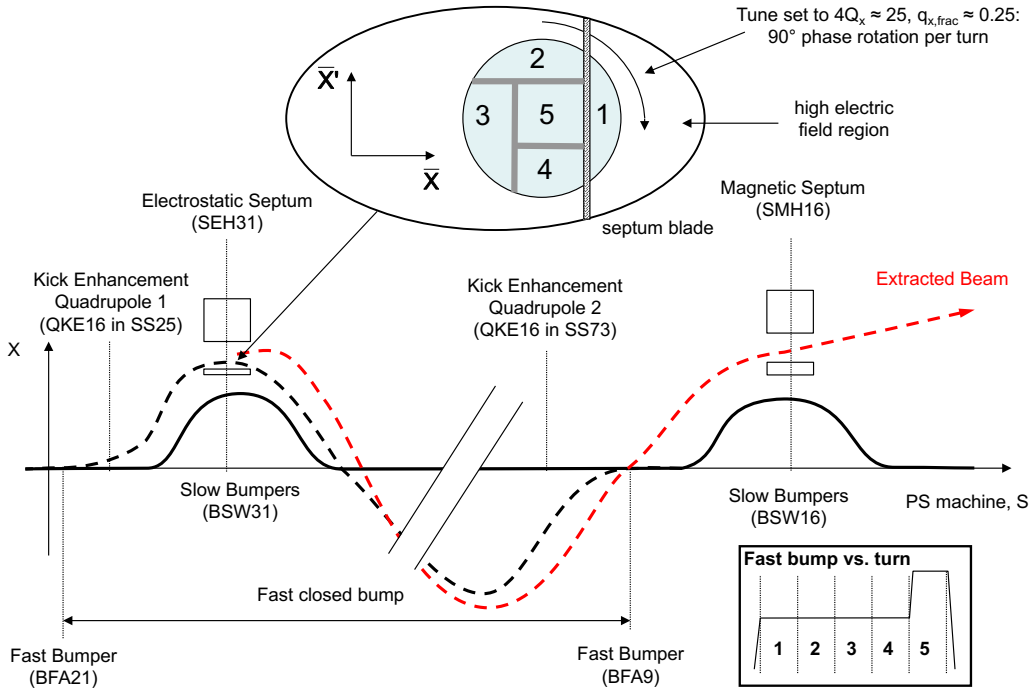

Fig. 16: Overview of CT extraction scheme at CERN PS: the numbers indicate the turn on which each slice is extracted.

A simplified waveform of the fast bump amplitude is shown in the bottom-right panel of Fig. 16, where in reality some turn by turn adjustment is available to help tune the spill by changing the presentation of the circulating beam to the electrostatic septum. In Fig. 17, an operational example of the BFA9 and 21 kicker waveforms used to control the fast bump around the SEH31 is presented, where the time-of-flight delay between the kickers located at different positions around the ring is evident. The relatively large number of turns makes the kicker system complex; more details of the kicker hardware used to produce such a turn by turn, variable amplitude closed bump can be found in Refs. [27, 28].

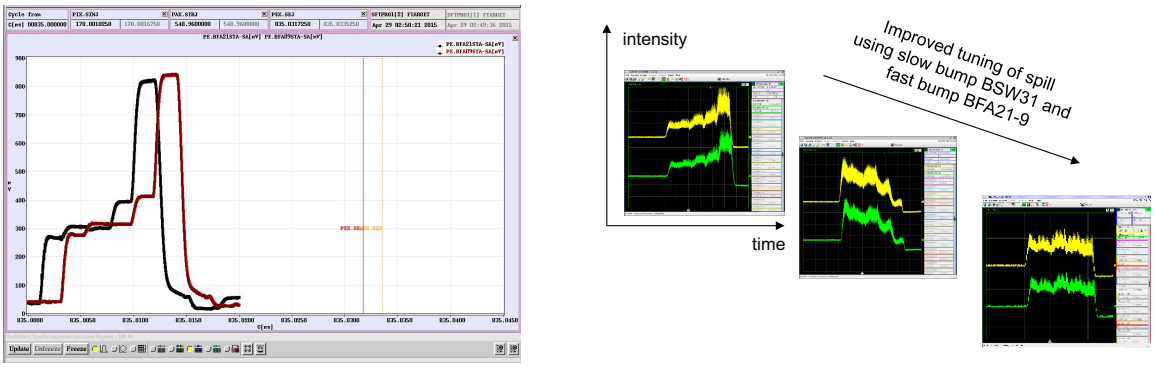

(a) BFA9 and 21 waveforms (b) Beam intensity extracted over five PS turns (10.5 µs)

Fig. 17: Turn by turn tuning of fast bumpers around SEH31 to achieve a spill with uniform intensity [29]

4.1.1.1 Turn by turn mismatch and trajectory error

A turn by turn variation in the position and emittance of each slice is observed in the extraction beam line and receiving machine as a result of tuning for constant intensity over the spill. This is illustrated at the electrostatic septum in Fig. 18. The resulting trajectory oscillations can be compensated by fast-pulsed, turn by turn kickers installed in the extraction beam line; however, the turn by turn optical mismatch is far more challenging to correct and is left uncorrected [30]. The turn by turn mismatch between the PS and SPS has been studied analytically for Gaussian and quasi-parabolic transverse distributions and for two cases: tuning the fast bump to maintain (i) constant intensity and (ii) constant emittance throughout the spill [22]. The results of this study are summarized in Fig. 19 for a Gaussian transverse distribution. The blow-up factor from mismatch for each turn is typically very high (30–50%) and smaller when holding the extracted intensity constant. In both cases, the average emittance, even after filamentation in the SPS, is considerably reduced compared with the emittance before CT extraction in the PS. This effect, resulting from the slicing of the phase-space into smaller pieces, has been exploited at CERN to overcome the vertical aperture limitation of the SPS by exchanging the horizontal and vertical emittances in the transfer line upstream of the SPS injection point. Such a phase-space manipulation is achieved using an insertion region containing normal and skew quadrupoles [31].

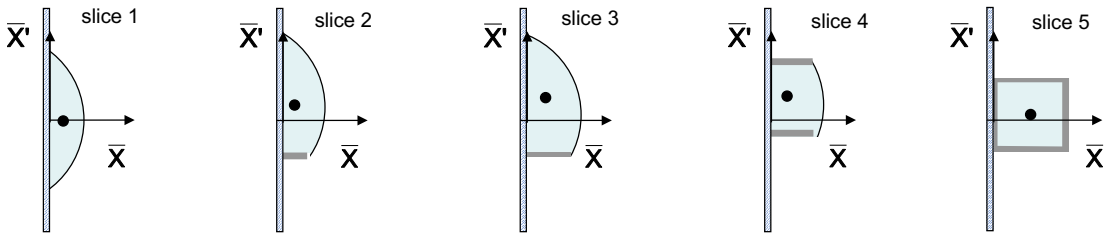

Fig. 18: Turn by turn centroid variation of slices extracted by CT

4.1.1.2 Beam loss during extraction and mitigation techniques

Depending on how well the extraction has been set up and optimized, approximately 6% of the beam is lost in the machine during the CT extraction process as it impinges and scatters from the electrostatic septum blade. Typically, one strives for a large β-function at the septum with as thin a blade as possible to reduce the amount of beam intercepted. The 1.8 m long SEH31 blade, composed of a molybdenum

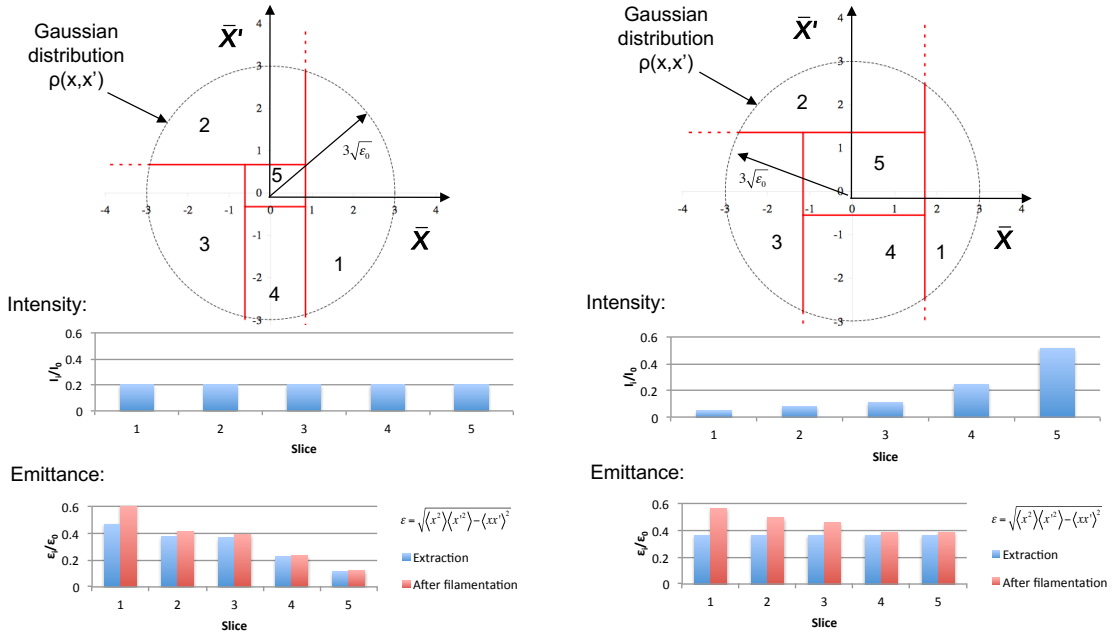

(a) Constant intensity per slice $= I_0/5$

(b) Constant emittance per slice $\neq \epsilon_0/5$

Fig. 19: Turn by turn intensity and emittance at extraction and after filamentation from mismatch in SPS [22]

foil, has a nominal thickness of 0.1 mm but warping of the foil caused by beam-induced heating typically increases its effective thickness over time. The magnitude of the β-function at the septum is limited by the gap width for the extracted beam over which the available high voltage must be applied to provide the electric deflection needed to jump the magnetic septum. The most critical parameter determining the extraction efficiency for CT is the relative alignment of the beam and septum, followed by the horizontal beam size (emittance) and the thickness of the septum blade; a complete explanation of the optimization of beam loss for CT can be found in Refs. [32, 33].

The loss distribution around the ring depends strongly on the optics and aperture of the machine. During high-intensity CNGS operation, these losses amounted to more than 1×10^{18} protons per year, which, at 14 GeV/c, induced significant radio-activation of the machine. This is especially problematic when localized on the extraction septa and makes hands-on maintenance difficult. The losses in the ring have also proven problematic where they arise at aperture restrictions located in regions of the PS with less shielding. The loss distribution around the ring for CT is presented in Fig. 25(b). For this reason, the loss distribution in the machine induced by primary beam scattering on the SEH31 has been studied in detail [26]. During the CNGS run, the optics of the machine had to be changed by moving the position of the QKE to displace the losses induced by the extraction into better-shielded parts of the ring.

The rise time of the kickers creating the fast bump and sweeping the beam over the electrostatic septum is not particularly important for the extraction efficiency, even though there is no particle-free gap in the circulating beam, because the losses are dominated by the transverse shaving process. A 30 cm passive array of tungsten wires is installed directly upstream of the SEH31 to reduce the beam loss on the electrostatic septum by inducing scattering and reducing the beam density on the downstream septum foil. This technique is commonly applied; the device is typically called a diffuser or scatterer [34–38].

For ambitious future beam intensities [39], the induced radioactivity poses a potential limit for the total intensity throughput of the CERN accelerator complex, potentially limiting the beam availability for the LHC. If the induced radioactivity is too high, lengthy cool-down periods would be imposed

before personnel could safely work on and repair the machine, impacting the availability in the event of inevitable failures. It was such concerns that motivated the development of magnetic splitting to boost the extraction efficiency and reduce the activation of the machine.

4.2 Resonant multiturn extraction: magnetic splitting

A beam can be split in transverse phase-space by capturing particles around separate, stable fixed points, or islands, created by non-linear magnetic fields applied as the betatron tune is moved slowly through a resonance. Particles captured around the stable fixed points are drawn away from the core of the beam by careful manipulation of the tune to physically split the beam. The concept of magnetic splitting removes the need to mechanically shave the beam on an electrostatic septum and can reduce the beam lost in the extraction process. In addition, the optical parameters of the extracted island are constant, turn by turn, at the extraction point and, as a consequence, the matching to the downstream machine can be better controlled with respect to shaving [22]. The extraction technique has been pioneered at CERN over the last two decades and has recently become the operational technique to extract proton beams from the PS destined for the SPS fixed-target physics programme [20, 40, 41]. Many splitting experiments have taken place in the PS over the years for different-order resonance crossings, including the third-order unstable resonance, as well as the fourth- and fifth-order stable resonances, splitting the beam into three, five, and six beamlets, respectively [42]. The fourth-order configuration was identified as operationally relevant as the splitting mechanism to replace CT and pursued further at CERN under the name 'multiturn extraction' (MTE). Readers may be particularly interested by the videos of the different splitting and capture processes collected on the CERN MTE team's website [43].

4.2.1 Non-linear dynamics: splitting and capture

A detailed treatment of non-linear dynamics is beyond the intended scope of this contribution, nevertheless, a very brief overview will be given to help introduce the extraction concept. For more information on the subject, the reader is invited to read further, e.g., Refs. [44, 45]. The past proceedings of the advanced accelerator physics courses of the CERN Accelerator School provide a particularly relevant resource on the subject, e.g., Ref. [46]. Non-linear dynamics is essentially concerned with the solution of the following equation of motion:

$$\frac{\mathrm{d}^2\bar{X}}{\mathrm{d}\mu^2} + Q^2\bar{X} = -Q^2\beta^{3/2}\frac{\Delta B(\bar{X},\mu)}{B\rho}\,, \tag{16}$$

where $(\bar{X}, \mu)$ are the canonical phase-space variables of normalized displacement and phase advance of a charged particle along the reference trajectory of the synchrotron, β is the betatron function, Q the tune, and $B\rho$ its magnetic rigidity. Many mathematical tools exist to help solve this differential equation, such as the Hamiltonian, Taylor maps, and Lie algebra, along with perturbation theory, normal form analysis, etc. This well-known equation of motion represents driven simple harmonic motion, where the source of the driving term on the right-hand side consists of linear (dipole and quadrupole) imperfections, as well as non-linear imperfections (sextupole, octupole, and so on), which can be expanded in terms of the magnetic multipole coefficients $b_n(\mu)$ present in the synchrotron:

$$\frac{\Delta B(\bar{X},\mu)}{B\rho} = \frac{B_0}{B\rho}\Big[b_0(\mu) + \beta^{1/2}b_1(\mu)\bar{X} + \beta b_2(\mu)\bar{X}^2 + \beta^{3/2}b_3(\mu)\bar{X}^3 + \dots\Big]\,. \tag{17}$$

It is these driving terms that perturb the circular particle trajectories in normalized phase-space; they become quickly significant to the beam stability when the frequency of the multipole terms drive a resonant condition with the tune of the synchrotron.

Solving the equation of motion numerically with a few lines of computer code will suffice here for the level of insight required. This can be achieved by constructing a Hénon-like map to model the

transverse dynamics, as is detailed at length in Ref. [47]. One can track a particle in the horizontal plane from turn n to turn $n+1$ by approximating the motion of each turn by a tune-dependent linear one-turn map followed by a thin lens multipole kick,

$$\begin{pmatrix} \bar{X} \\ \bar{X}' \end{pmatrix}_{n+1} = R_{1-\text{turn}}(2\pi Q) \begin{pmatrix} \bar{X} \\ \bar{X}' + K_2\bar{X}^2 + K_3\bar{X}^3 + \ldots \end{pmatrix}_n , \tag{18}$$

where K_n are integrated normalized multipole strengths and $K_0 = K_1 = 0$ in this case. Of course, for MTE, the imperfections are voluntarily applied to drive the splitting. Different normalizations are commonly applied in accelerator physics; one will see special adimensional normalized co-ordinates applied in most of the MTE literature to better elucidate the ratio of the sextupole and octupole strengths.

The concept employed at the PS is demonstrated in Fig. 20 for a horizontal fourth-order resonance crossing in the presence of sextupole and octupole magnetic fields, where 12 particles are initialized and tracked over 1000 turns. In this example, the dynamics is linear at small amplitudes before the tune is swept up through the resonance and four stable fixed points are created in addition to the one at the origin. The fixed points move away from the core as the tune distance above the resonance is increased, until two distinct regions in phase-space are formed: the core and four islands. The phase-space plots in Fig. 20 were created by iterating the map at different values of Q, K_2, and K_3. Islands are formed at the fourth-order resonance crossing even without octupole fields, i.e., with $K_3 = 0$; however, the introduction of octupoles provides another degree of freedom to better adjust the splitting and capture process, allowing better control of the tune and size of the islands, along with many other important parameters. The differences in the size, shape, and position of the islands with $K_3 = 0$ are demonstrated in Fig. 21. A Hamiltonian description of the process can be found in Ref. [48], where it is used to describe analytically how the position and size of the stable fixed points change as a function of the multipole strengths, as well as give an understanding of the non-linear contributions to the tune. Further details of the numerical simulations carried out and benchmarked to design and commission the MTE at the CERN PS can be found in Refs. [49–53].

The uniformity of the extracted spill depends directly on how evenly the beam intensity, which is initially located in the beam core, is shared and re-distributed between the core and the islands during the splitting process. The splitting efficiency is used as a figure-of-merit to parametrize the performance of MTE and is defined as

$$\eta_{\text{MTE}} = \frac{\langle I_{\text{islands}} \rangle}{I_{\text{total}}} , \tag{19}$$

where $\langle I_{\text{islands}} \rangle$ and I_{total} stand for the average intensity in the islands and the total beam intensity, respectively. The requirements of the SPS specify that the spill must be uniform to $\pm 1\%$ of the total intensity per turn, i.e., $\eta_{\text{MTE}} = (20 \pm 1)\%$ for a splitting over five turns. Unlike CT, the uniformity of the spill is predetermined by the splitting efficiency before the actual fast extraction process is initiated. The size of the beam core (horizontal emittance) before splitting has a significant impact on the splitting efficiency [20]. Excitation from the transverse damper is applied to the beam to increase the emittance of the core during resonance crossing and help improve the intensity distribution among the beamlets formed during the splitting and capture process. The role played by transverse excitation in the splitting and capture process is a topic of active research [53].

After acceleration and on the flat-top at 14 GeV/c, the non-linear sextupole and octupole fields are applied before the tune is swept adiabatically (slowly) through the fourth-order resonance at $4Q_x = 25$ to start the splitting and capture process. To minimize the perturbation to the tune from the longitudinal plane, the chromaticity is held close to zero and the momentum spread of the beam reduced by significantly reducing the RF voltage. The splitting efficiency is significantly degraded without reducing the momentum spread in the beam; in this way, most particles cross resonance together. Careful control of the machine is needed throughout the splitting process and especially in the presence of the non-linear fields applied. The stability and reproducibility of the machine was one of the main challenges

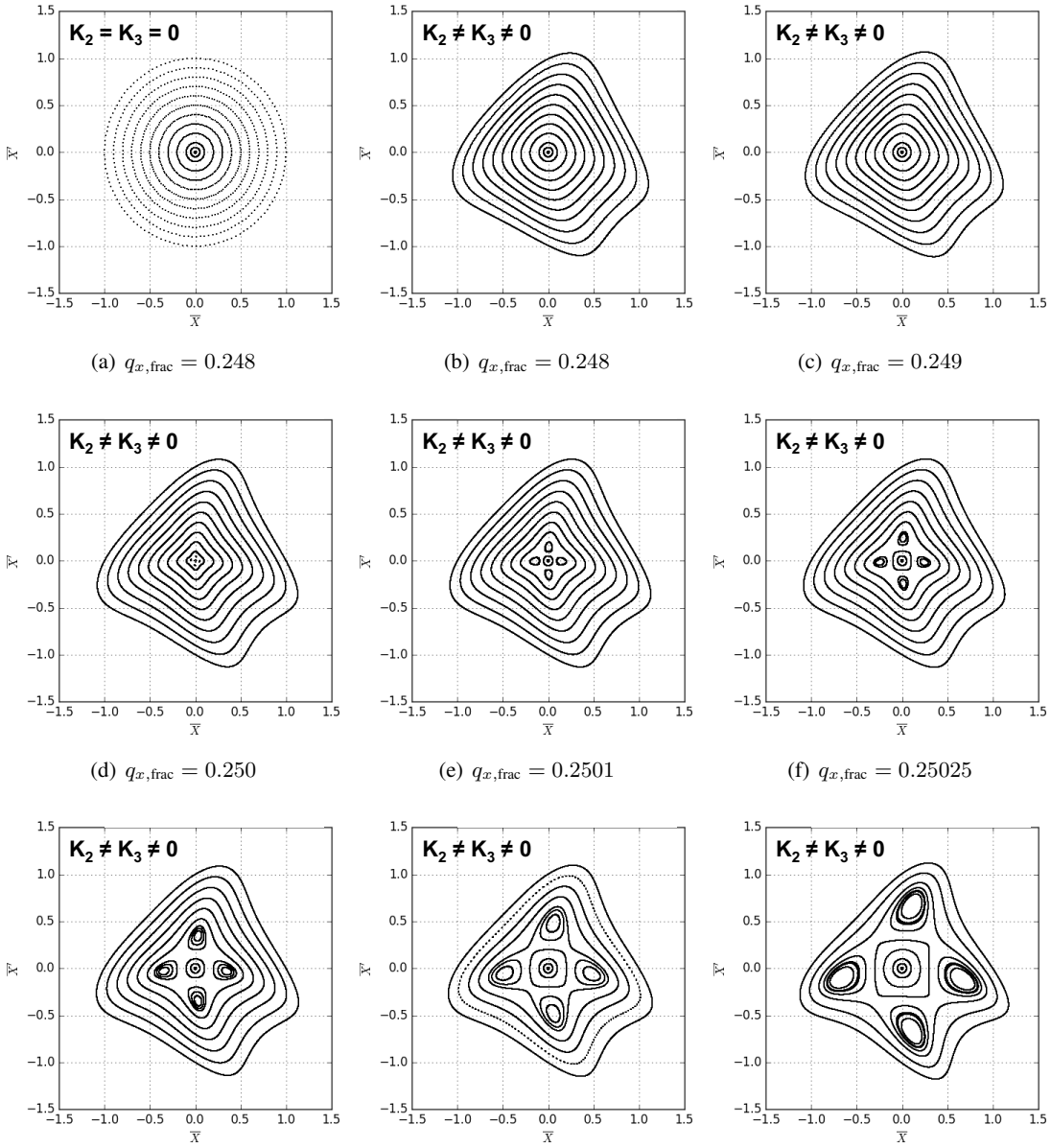

(a) $q_{x,\text{frac}} = 0.248$ (b) $q_{x,\text{frac}} = 0.248$ (c) $q_{x,\text{frac}} = 0.249$

(d) $q_{x,\text{frac}} = 0.250$ (e) $q_{x,\text{frac}} = 0.2501$ (f) $q_{x,\text{frac}} = 0.25025$

(g) $q_{x,\text{frac}} = 0.2505$ (h) $q_{x,\text{frac}} = 0.251$ (i) $q_{x,\text{frac}} = 0.252$

Fig. 20: Phase-space portraits of 12 particles tracked over 1000 turns by a Hénon-like mapping in the presence of a thin lens sextupole and octupole ($K_2 \neq K_3 \neq 0$) as the tune is swept across the horizontal fourth-integer resonance from $q_{x,\text{frac}} = 0.248$ to 0.252. The multipole is initially turned off (a) before being turned on and held constant as the tune is swept from (b) to (i).

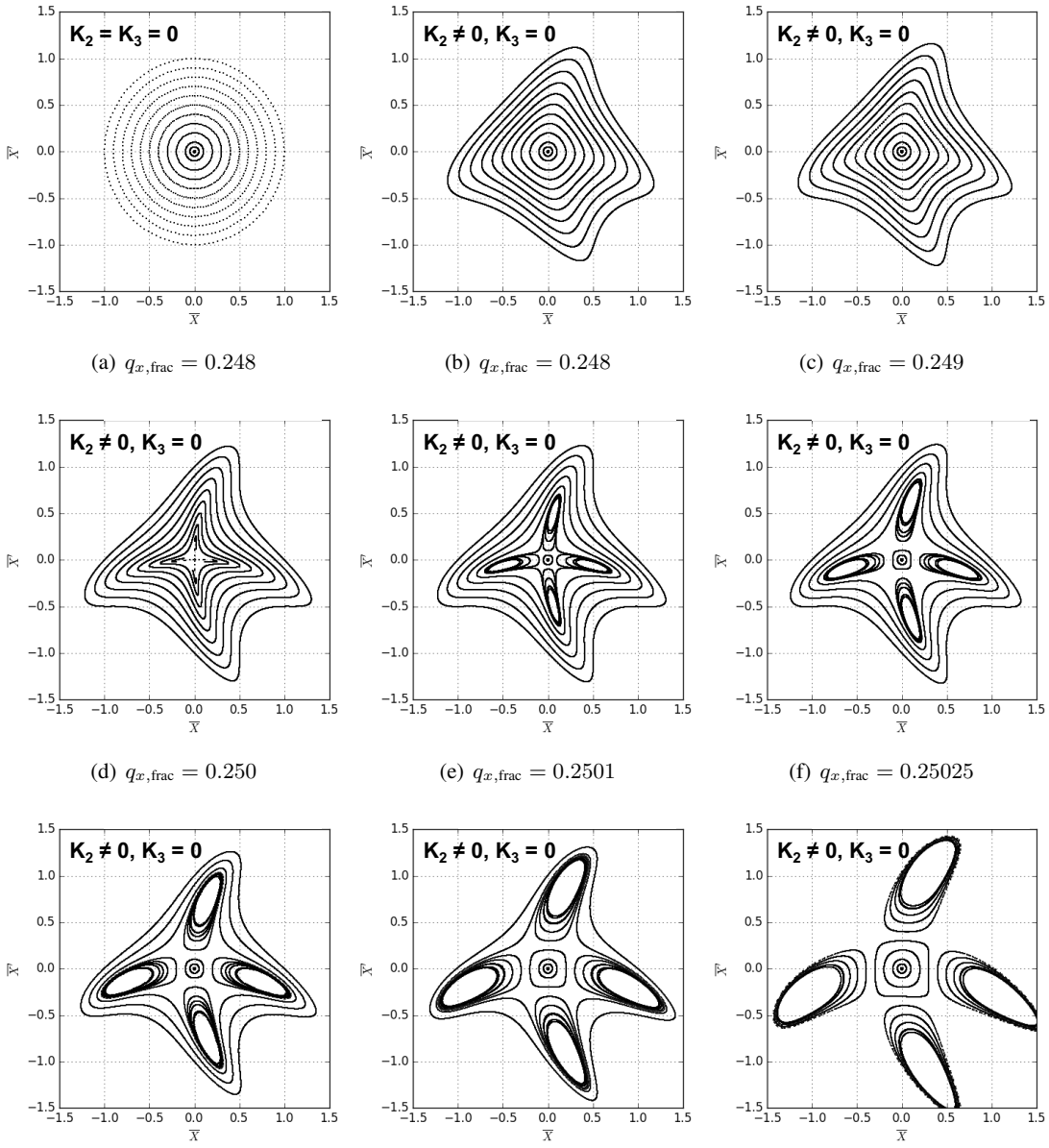

(a) $q_{x,\text{frac}} = 0.248$ (b) $q_{x,\text{frac}} = 0.248$ (c) $q_{x,\text{frac}} = 0.249$

(d) $q_{x,\text{frac}} = 0.250$ (e) $q_{x,\text{frac}} = 0.2501$ (f) $q_{x,\text{frac}} = 0.25025$

(g) $q_{x,\text{frac}} = 0.2505$ (h) $q_{x,\text{frac}} = 0.251$ (i) $q_{x,\text{frac}} = 0.252$

Fig. 21: Phase-space portraits of 12 particles tracked over 1000 turns by a Hénon-like mapping in the presence of a thin lens sextupole ($K_2 \neq 0$, $K_3 = 0$) as the tune is swept across the horizontal fourth-integer resonance from $q_{x,\text{frac}} = 0.248$ to 0.252. The multipole is initially turned off (a) before being turned on and held constant as the tune is swept from (b) to (i).

that the MTE team faced in realizing the novel extraction scheme. Once the islands are formed, they are rotated in phase-space by manipulation of the multipole strengths to optimize the physical separation presented to the extraction septum [52]. Before extraction, the beam is debunched and partially recaptured at 200 MHz, as previously done for CT.

4.2.2 Extraction process

A detailed overview of the implementation of the MTE equipment installed in the PS, including the dedicated multipole magnets and extraction equipment, can be found in Ref. [20]. During the splitting process, the beam is separated into two distinct regions in horizontal phase-space: the core and the islands, which circulate on separate closed orbits in the machine. The core of the beam sits on the reference closed orbit, as it did before the splitting was initiated, and the islands circulate on another closed orbit, which loops around the machine four times before closing on itself. The beam captured in the islands represents a continuous entity (if the beam is debunched) that also snakes around the machine, as depicted by the well-known plot in Fig. 22. One would observe a test particle trapped in the islands at a given location in the ring jump from one island to the next as it returns and is rotated by the fractional tune $q_{x,\text{frac}} \approx 0.25$ each turn.

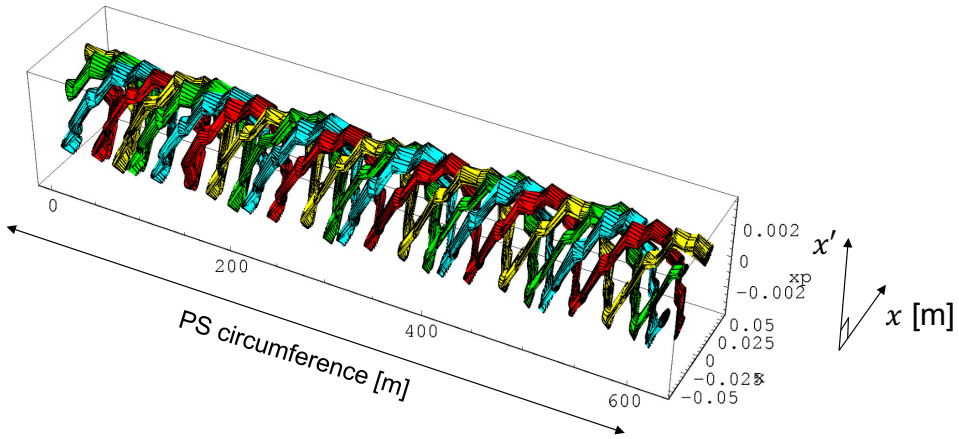

Fig. 22: Islands looping and rotating with the phase advance around the circumference of the PS four times, connected continuously into one single entity, where each island, or turn, is represented by a different colour [20].

After splitting and capture, a slow bump brings the circulating beams close to the septum before the extraction is initiated by a fast, closed bump pushing one island over the septum blade, as shown in Fig. 23. Most notably, an electrostatic septum is not required and a single magnetic extraction septum can be used, which in this case is the SMH16 mentioned previously. The tune rotates the rest of the beam, snaking around the machine into the septum aperture during the subsequent four turns, which parallels the CT extraction process described previously. A classic fast extraction is employed to extract the core on the fifth turn. Figure 23 also demonstrates clearly how the optical parameters of the island pushed over the septum blade stay constant throughout the extraction. The extraction kicker scheme used for MTE is summarized in Fig. 24.

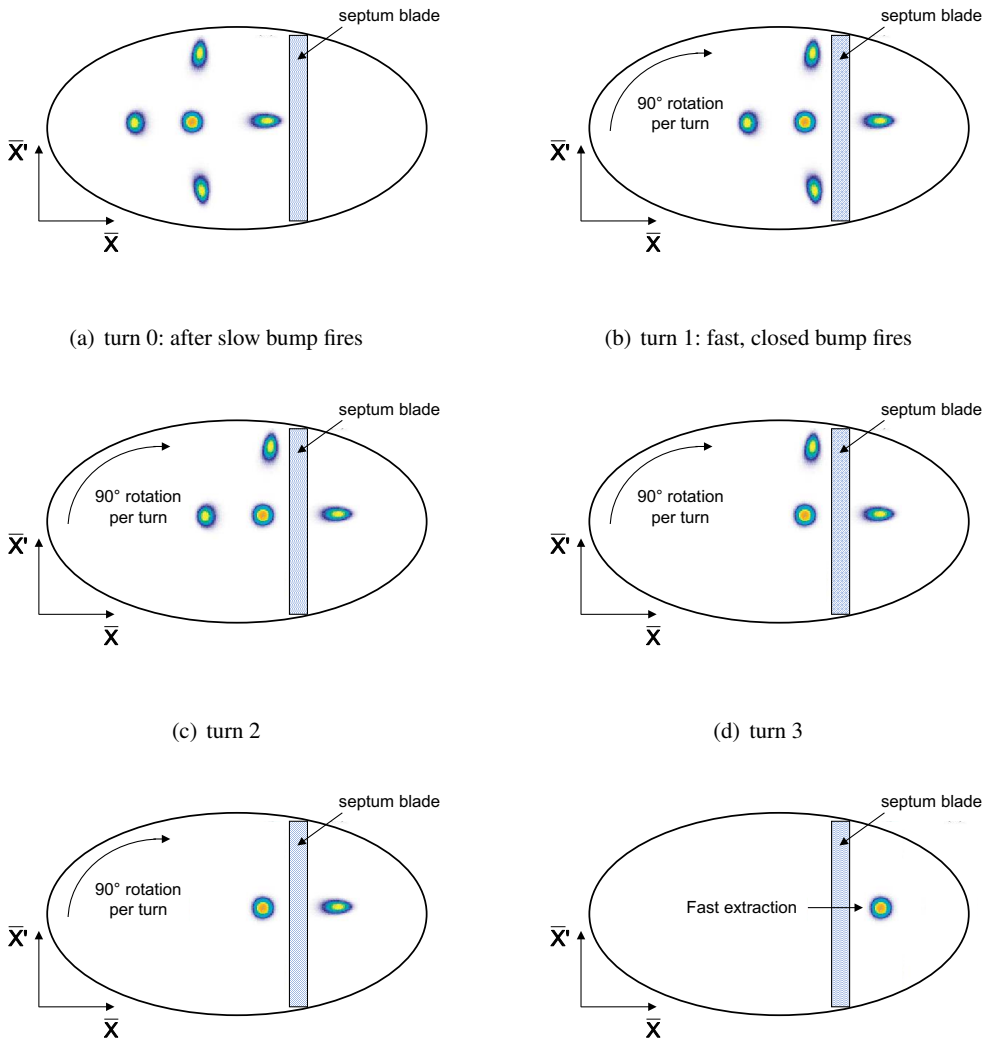

(a) turn 0: after slow bump fires

(b) turn 1: fast, closed bump fires

(c) turn 2

(d) turn 3

(e) turn 4

(f) turn 5: fast extraction

Fig. 23: Turn by turn phase-space diagram of the MTE extraction process at the location of the extraction septum, SMH16.

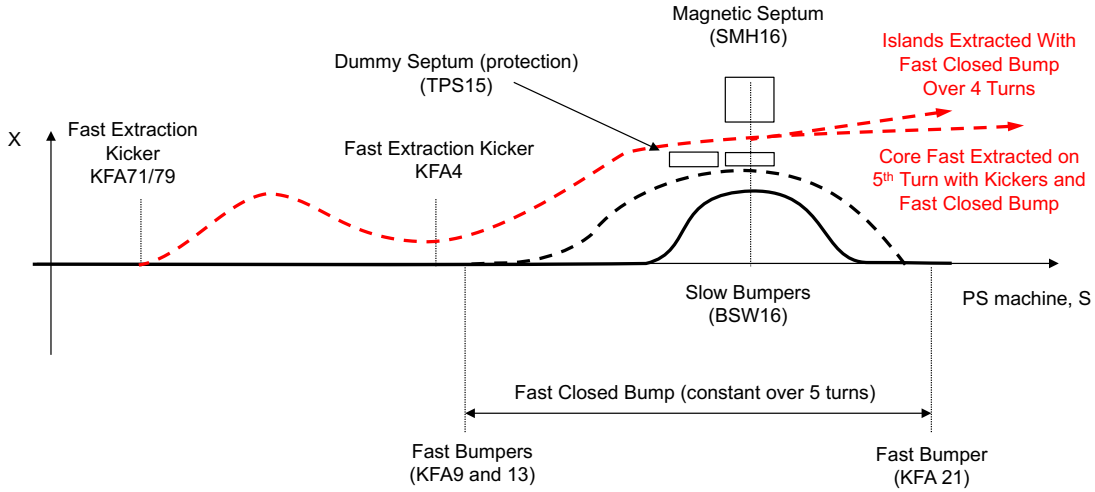

Fig. 24: Overview of the MTE extraction scheme at the CERN PS. The second fast kicker (KFA4) is used to correct the extraction trajectory of the core and minimize the difference with respect to the islands.

4.2.3 Beam loss

The MTE extraction process would be essentially loss-free in the presence of a longitudinal particle-free gap in the circulating beam because the transverse splitting and capture losses can be kept very low. Unfortunately, the beam must be debunched around the circumference of the PS to satisfy the requirements of the SPS and, as a result, beam is lost on the extraction septum as the beam is swept across its blade during the rise of the fields of the fast-pulsed kicker systems, both when the fast, closed bump is fired to extract the islands and when the core is fast-extracted. In contrast with CT, the rise times of the kicker systems involved are critical in minimizing the beam loss. To protect the SMH16, a water-cooled copper absorber was installed in the upstream straight section to absorb the majority of the beam energy that would otherwise have directly impacted the septum blade. The absorber, which resembles a passive septum blade and is commonly known as the 'dummy' septum or the TPS15, is the location in the ring at which most of the losses occur during the MTE process. Further details of the TPS15 can be found in Ref. [54]. The typical beam loss signal measured close to the extraction region is shown in Fig. 25(a). The difference in the rise times of the fast, closed bump (islands) and fast extraction (core) systems is evident in the magnitude of the loss signals.

The integrated beam loss monitor signals recorded during extraction around the PS ring for CT and MTE are compared in Fig 25(b). The MTE losses are far more localized close to the extraction region and, in particular, the TPS15, which allows the beam-induced activation of the machine to be more effectively shielded. The losses on aperture bottlenecks in the ring created during CT by beam scattering from the SEH31 largely disappear. Radiation survey measurements made approximately 30 hours after operation of CT or MTE reflect the change in the prompt extraction beam loss monitor profile, as presented in Fig. 26.

The implementation of MTE at the PS has improved the extraction losses by about a factor of three compared with CT, reducing from approximately 6% to less than 2%, despite the beam being debunched. The extraction efficiency for CT is compared with that for MTE during 2015 in Fig. 27, where the extraction efficiency is shown to be relatively insensitive to the beam intensity. Ways to reduce the fast, closed bump rise time and to implement a particle-free gap, perhaps via the barrier bucket technique [56], are being considered to further reduce the extraction losses.

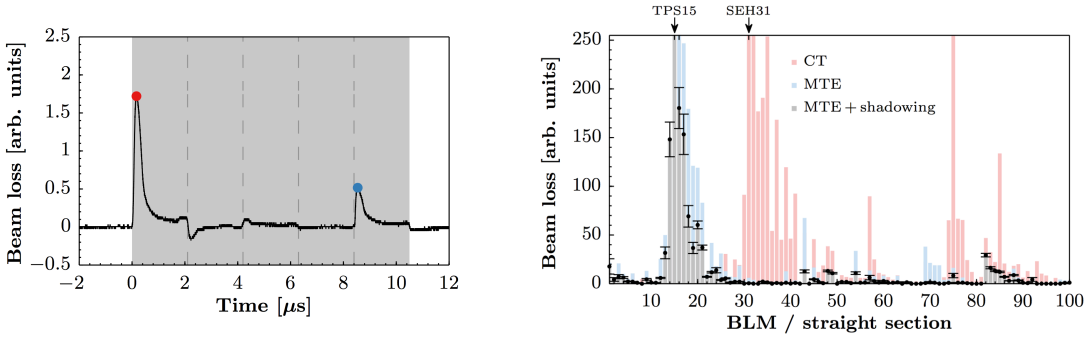

(a) At TPS15 for MTE: red, islands; blue, core

(b) At extraction around the PS ring and compared with CT

Fig. 25: Beam loss monitor (BLM) signals during extraction for MTE: the beam is swept across the septum blade as the fast-pulsed magnets fire [52].

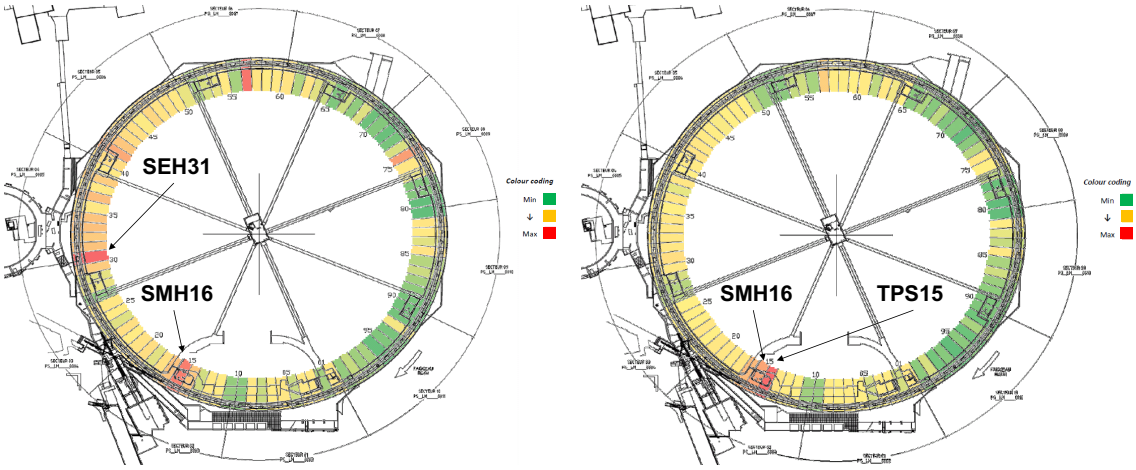

(a) After CT operation: end of 2014

(b) After MTE operation: end of 2015

Fig. 26: Radioactive dose distribution around the PS ring with MTE measured approximately 30 hours after operation [55].

4.2.4 Operational challenges

The MTE splitting process is resonant and sensitive to even very small changes in the magnetic reproducibility of the machine. An example of a bad spill is shown in Fig. 28, where the intensity over the five turns is shown alongside a beam profile measurement made using a wire-scanner device. The poor splitting efficiency in this case is clearly observed by the overpopulation of the core shown in both the spill and the profile measurements.

An important step in making MTE operational at the PS was to understand the different factors affecting the stability of the machine. In particular, periodic fluctuations in the splitting efficiency could be correlated to low frequency noise (at 5 kHz) of unsynchronized power converters driving the magnetic circuits used to control the tune and chromaticity of the PS. The resulting tune modulation caused oscillations in the splitting efficiency with a time period of the order of tens of minutes. With the power converters synchronized and the ripple reduced, the machine reproducibility and splitting efficiency was significantly improved. Detailed beam dynamics simulations were also carried out to understand the phenomenon and the frequency dependence of the tune ripple. Further details of this work can be found

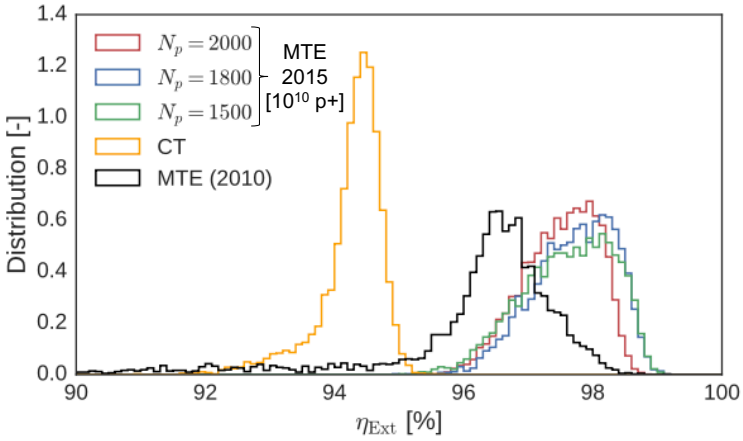

Fig. 27: MTE extraction efficiency compared with CT [40]

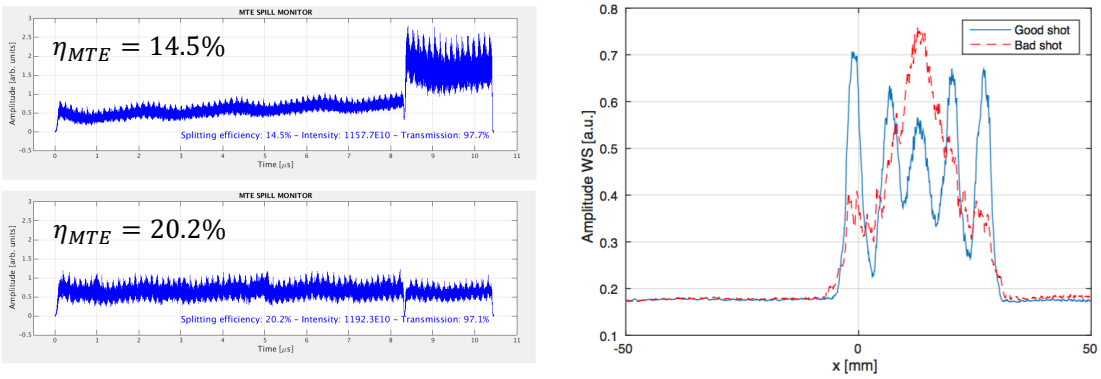

(a) Spill intensity as function of time: upper, bad shot; lower, good shot.

(b) Wire-scanner profile comparison for the same two shots.

Fig. 28: Example of a good spill compared with a bad spill following a change in machine reproducibility [40]

in Ref. [53]. It should be noted that the application of transverse damper excitation during splitting is imperative to increase the capture probability during island formation and reduce its sensitivity to the initial horizontal emittance. One major drawback of MTE at CERN is that the beam emittance in the plane of extraction is not significantly reduced compared with the initial emittance, as it is in the case of the shaving employed for CT. Without the possibility of reducing the vertical emittance through phase-space exchange in the transfer line between the PS and SPS, the larger vertical emittance seen by the SPS with MTE results in poorer transmission. Work is actively ongoing to create and preserve smaller vertical emittance throughout the CERN accelerator chain and throughout the MTE cycle in the PS. The future charge-exchange injection scheme foreseen in the PS booster will help reduce the vertical emittance in the longer term. There are many other operational issues too detailed for this paper that also required particular attention to realize the MTE scheme, e.g., mechanical aperture, operation of the PS in the presence of a dummy septum, impact of the slow bump on the tune, and turn by turn trajectory differences, to mention just a few. Further details can be read in the MTE Design Report [20].

Acknowledgement

The vast majority of the material in this contribution was provided by colleagues at CERN, in particular those from the ABP, ABT, and OP groups and especially the MTE team, with D. Cotte, B. Goddard, M. Giovannozzi, S. Gilardoni, A. Huschauer, and G. Sterbini requiring notable acknowledgement. A special, personal, thanks goes to A. Huschauer and F. Velotti for taking the time to review these proceedings.

References

[1] M. Benedikt and F. Zimmerman, Status of the future circular collider study, 25th Russian Particle Accelerator Conf., Saint Petersburg, 2016, CERN-ACC-2016-0331, p. TUYMH01.

[2] O. Brüning *et al.* (eds.), LHC design report v. 1: the LHC Main Ring, CERN-2004-003-V-1 (CERN, Geneva, 2004), https://doi.org/10.5170/CERN-2004-003-V-1.

[3] R. Bossart *et al.*, *IEEE Trans. Nucl. Sci.* **16** (1969) 286, https://doi.org/10.1109/TNS.1969.4325235.

[4] F.M. Velotti, Ph.D. thesis, Ecole Polytechnique Lausanne, CERN-THESIS-2017-041, 2017.

[5] M.A. Fraser *et al.*, Experimental results of crystal-assisted slow extraction at the SPS, 8th International Particle Accelerator Conf., Copenhagen, 2017, p. MOPIK048.

[6] V. Forte *et al.*, Beam-based kicker waveform measurements using long bunches, 8th International Particle Accelerator Conf., Copenhagen, 2017, p. MOPIK042.

[7] F. Velotti *et al.*, Performance studies of the SPS beam dump system for HL-LHC beams, CERN 5th International Particle Accelerator Conf., Dresden, 2014, CERN-ACC-2014-0239, p. THPME069.

[8] C. Wiesner *et al.*, LHC beam dump performance in view of the high luminosity upgrade, 8th International Particle Accelerator Conf., Copenhagen, 2017, p. WEPIK033.

[9] M.J. Barnes and B. Goddard, Considerations on a new fast extraction kicker concept for SPS, CERN-sLHC-Project-Note-0018, (CERN, Geneva, 2010).

[10] S. Gilardoni and D. Manglunki (eds.), Fifty years of the CERN Proton Synchrotron: vol. 1, CERN-2011-004 (CERN, Geneva, 2011), https://doi.org/10.5170/CERN-2011-004.

[11] K. Wille, *The Physics of Particle Accelerators: An Introduction* (Oxford University Press, Oxford, 2000).

[12] H. Wiedemann, *Particle Accelerator Physics*, 3rd ed. (Springer, Berlin, 2007).

[13] `http://mad.web.cern.ch/mad`, last accessed January 18th 2018.

[14] V. Mertens, Protons on the doorstep of the LHC, *CERN Courier*, 1 March 2005. `http://cerncourier.com/cws/article/cern/29275`.

[15] M. Benedikt *et al.* (eds.), LHC design report v. 3: the LHC injector chain, CERN-2004-003-V-3 (CERN, Geneva, 2004), https://doi.org/10.5170/CERN-2004-003-V-3.

[16] J. Borburgh *et al.*, Upgrade of the CERN SPS extraction protection elements TPS, 6th International Particle Accelerator Conf., Richmond, Va., 2015, CERN-ACC-2017-0020, p. WEPMN068.

[17] B. Goddard, Fast extraction from SPS LSS4 for the LHC and NGS projects, SL-Note-98-066-SLI, (CERN, Geneva, 1998).

[18] V. Kain *et al.*, High intensity commissioning of SPS LSS4 extraction for CNGS, 22nd Particle Accelerator Conf., Albuquerque, N.M., 2007, CERN-AB-2007-048, p. TUPAN096, https://doi.org/10.1109/PAC.2007.4440837.

[19] W. Bartmann *et al.*, Beam transfer to the FCC-hh collider from a 3.3 TeV booster in the LHC tunnel, IPAC2015, Richmond, Va., CERN-ACC-2015-012, p. THPF089.

[20] M. Giovannozzi (ed.), The CERN PS multi-turn extraction based on beam splitting in stable islands of transverse phase space: design report, CERN-2006-011 (CERN, Geneva, 2006), https://doi.org/10.5170/CERN-2006-011.

[21] K.H. Reich, Decaturn beam extraction for synchrotrons, accelerator department internal report BNL-AADD-100, BNL, N.Y., 1966.

[22] R. Cappi and M. Giovannozzi, Computation of betatron mismatch and emittance blow-up for multi-turn extraction, CERN/PS 2002-083 (AE) (CERN, Geneva, 2002).

[23] V.D. Rudko *et al.*, *Instrum. Exp. Tech.* **59** (2016) 325, https://doi.org/10.1134/S0020441216020330.

[24] M. Gyr and E.B. Vossenberg, Half-integer fast resonant extraction with quasi rectangular spill, 3rd European Particle Accelerator Conf., Berlin, 1992, p.1501.

[25] C. Bovet *et al.*, The fast shaving ejection for beam transfer from the CPS to the CERN 300 GeV machine, 5th IEEE Particle Accelerator Conf., San Francisco, 1973 [IEEE Trans. Nucl. Sci. **20** (1973) 438], https://doi.org/10.1109/TNS.1973.4327144.

[26] J. Barranco Garcia and S. Gilardoni, *Phys. Rev. ST Accel. Beams* **14** (2011) 030101. https://doi.org/10.1103/PhysRevSTAB.14.030101.

[27] D. C. Fiander *et al.*, A modulated fast bump for the CPS continuous transfer, Accelerator Conf., Chicago, 1977 [IEEE Trans. Nucl. Sci. **24** (1977) 1340], https://doi.org/10.1109/TNS.1977.4328938.

[28] L. Sermeus, MTE/CT ABT systems: past and present, ABT Engineering Forum, CERN, Geneva, 2018, `https://indico.cern.ch/event/685066/`.

[29] D. Cotte, MTE at PS: considerations from OP, MTE Internal Review, CERN, Geneva, 2015.

[30] A. Franchi *et al.*, Trajectory correction in the transfer line TT2-TT10 for the continuous transfer (CT), CERN-AB-Note-2008-005, (CERN, Geneva, 2007).

[31] L.R. Evans, A phase plane exchange section for the SPS antiproton injection beam-line, CERN-SPS-DI-MST-80-2 (CERN, Geneva, 1980).

[32] M. Giovannozzi, Comparison of extraction losses for present CT and novel multi-turn extraction, APC Meeting, 2005.

[33] M. Giovannozzi, Follow-up of comparison of extraction losses for present CT and novel multi-turn extraction, APC Meeting, 2005.

[34] C. Germain *et al.*, Technical developments of the CERN electrostatic program, 2nd International Symposium on Insulation of High Voltages in Vacuum, Boston, Mass., 1966, p. 279.

[35] M. Thivent, Developpements lies a la construction des deflecteurs electrostatiques, PS/PSR/Note 83-8, (CERN, Geneva, Switzerland), 1983.

[36] A. Durand, Efficacite d'un reseau de fils place devant la plaque du septum du transfert continue à 12 GeV/c, University de Rennes, France, 1974.

[37] A. Durand, Sur la diffusion de protons de $p = 400$ GeV/c par un reseau de fils place devant la plaue d'un septum electrostatique, University de Rennes, France, 1974.

[38] B. Goddard *et al.*, The use of a passive scatterer for SPS slow extraction beam loss reduction, Proceedings IPAC'17, Copenhagen, 2017, p. MOPIK044.

[39] A. Golutvin *et al.*, A facility to search for hidden particles (SHiP) at the CERN SPS, CERN-SPSC-2015-016 (SPSC-P-350), (CERN, Geneva, 2015).

[40] S. Abernethy *et al.*, *Phys. Rev. Accel. Beams* **20** (2017) 014001. https://doi.org/10.1103/PhysRevAccelBeams.20.014001.

[41] A. Huschauer *et al.*, *Phys. Rev. Accel. Beams* **20** (2017) 061001. https://doi.org/10.1103/PhysRevAccelBeams.20.061001.

[42] A. Franchi *et al.*, *Phys. Rev. ST Accel. Beams* **12** (2009) 014001. https://doi.org/10.1103/PhysRevSTAB.12.014001.

[43] `https://ab-project-mte.web.cern.ch`, last accessed January 18th 2018.

[44] D.A. Edwards and M.J. Syphers, *An Introduction to the Physics of High Energy Accelerators*, (Wiley, New York, 2003).

[45] T.W.B. Kibble and F.H. Berkshire, *Classical Mechanics*, 5th ed. (Imperial College Press, London, 2004).

[46] W. Herr (ed.), CAS–CERN Accelerator School: Advanced Accelerator Physics Course, Trondheim, Norway, 18–29 August 2013, edited by W. Herr, CERN-2014-009 (CERN, Geneva, 2014), https://doi.org/10.5170/CERN-2014-009.

[47] A. Bazzani *et al.*, A normal form approach to the theory of nonlinear betatronic motion, CERN-94-02 (CERN, Geneva, 1994), https://doi.org/10.5170/CERN-1994-002.

[48] M. Giovannozzi and P. Scaramuzzi, Nonlinear dynamics studies at the CERN Proton Synchrotron: precise measurements of islands parameters for the novel multi-turn extraction, EPAC'04, Lucerne, 2004, p. 1861.

[49] R. Cappi and M. Giovannozzi, *Phys. Rev. Lett.* **88** (2002) 104801. https://doi.org/10.1103/PhysRevLett.88.104801.

[50] R. Cappi and M. Giovannozzi, *Nucl. Instrum. Meth. A* **519** (2004) 442. https://doi.org/10.1103/PhysRevLett.88.104801.

[51] S.Gilardoni *et al.*, *Nucl. Instrum. Meth. A* **561** (2006) 249. https://doi.org/10.1016/j.nima.2006.01.021.

[52] A. Huschauer, Ph.D. thesis, Technische Universität Wien, 2016, CERN-THESIS-2016-061.

[53] A. Huschauer *el al.*, Transverse beam splitting made operational: key features of the multiturn extraction at the CERN Proton Synchrotron, 57th ICFA Advanced Beam Dynamics Workshop on High-Intensity and High-Brightness Hadron Beams, 2016 [Phys. Rev. Accel. Beams **20** (2017) 061001].

[54] C. Bertone *et al.*, Studies and implementation of the PS dummy septum to mitigate irradiation of magnetic septum in straight section 16, CERN-ACC-2014-0043 (CERN, Geneva, 2008).

[55] G. Dumont, RP survey of PSB, PS and SPS, MSWG Meeting 2016 #2, (CERN, Geneva, 2016).

[56] H. Damerau, Ph.D. thesis, Technische Universität Damstadt, 2005, CERN-THESIS-2005-048.